Journal of Environmental Management 340 (2023) 117958

Contents lists available at ScienceDirect

Journal of Environmental Management

journal homepage: www.elsevier.com/locate/jenvman

Research article

Hydrogeological characteristics and water availability in the mountainous aquifer systems of Italian Central Alps: A regional scale approach

Stefania Stevenazzi [a], Chiara Zuffetti [b], Corrado A.S. Camera [b,*], Alice Lucchelli [b], Giovanni Pietro Beretta [b], Riccardo Bersezio [b], Marco Masetti [b]

[a] Dipartimento di Ingegneria Civile, Edile e Ambientale, Università degli Studi di Napoli Federico II, Piazzale Tecchio, 80, Naples, 80125, Italy
[b] Dipartimento di Scienze della Terra "A. Desio", Università degli Studi di Milano, Via Luigi Mangiagalli, 34, Milan, 20133, Italy

ARTICLE INFO

Keywords:
Groundwater body
Groundwater budget
Groundwater quality
Stable isotope analysis
Geological modelling
Italy

ABSTRACT

Groundwater resources in mountain areas are strategically important to maintain adequate water supply for domestic uses, farming, industrial activities, and energy production, also considering the expected growing demand due to ongoing climate changes. Within this framework, the objective of the study is to develop a regional approach, compliant with the European requirements of the Water Framework Directive 2000/60/EC and Groundwater Directive 2006/118/EC, that could support public agencies and water companies to efficiently manage and protect the available water resources in mountainous environments.

The proposed approach identifies and delineates groundwater bodies by coupling a 3D hydro-stratigraphic model with the definition of the water budget and water hydrochemical fingerprints in a geologically complex Alpine environment in Northern Italy. Sixteen groundwater bodies (GWBs) have been identified all over the 10.290 km^2 area, showing an average storage capacity of more than 500 $Mm^3\ y^{-1}$ (about 3% of the average total inflow from precipitation and snowmelt), with differences up to four times between GWBs mainly constituted of carbonate rocks and those prevalently composed of crystalline or terrigenous rocks. Groundwater quality in the study domain is generally excellent, with few exceptions due to geogenic (i.e., natural) or anthropogenic sources of contamination. The results of this study show the advantages of coupling 3D hydro-stratigraphic modelling combined with meteorological, hydrological and hydrogeological information, which consist in: i) identifying the most Strategic Storage Reservoir both in terms of quality and storage capacity; ii) evaluating the present ground- and surface water availability; iii) detecting areas of specific interest for implementing groundwater monitoring networks; iv) recognising recharge areas of the most relevant springs, to implement protection strategies of the resource.

1. Introduction

Mountains are a strategically important component of global water supply due to the combination of high precipitation and low evapotranspiration that allows the development of large storage of good groundwater quality efficiently recharged (Somers and McKenzie, 2020). Spring discharge in mountain and hilly areas is essential to maintain adequate water supply both for drinking supply and to other anthropogenic activities, including agriculture, industrial activity, and energy production, as well as to preserve the functionality of groundwater-dependent ecosystems (Dwire et al., 2018). Groundwater storage in Alpine regions is also essential for maintaining the baseflow in mountain streams (Christensen et al., 2020). Viviroli et al. (2020) estimate that water demand in mountain areas is growing and that 1.4 billion people will depend critically on mountain runoff by 2050. Groundwater in mountain environments is going to represent an asset in the increasing demand for clean and safe water in many areas of the world.

This groundwater is also an important resource to cope with climate modifications. Ferrer et al. (2012) highlight that climate changes in the Mediterranean area should make the amount of groundwater resources more vulnerable, due to predicted rise in temperature and reduction in precipitation, which should reduce the available water resources (Milly et al., 2005). However, even if mountain areas could be more sensitive to climate changes than lowlands (IPCC, 2019), Somers and McKenzie (2020) showed that the resiliency of groundwater can mitigate the

* Corresponding author.
E-mail address: corrado.camera@unimi.it (C.A.S. Camera).

https://doi.org/10.1016/j.jenvman.2023.117958
Received 4 November 2022; Received in revised form 17 February 2023; Accepted 14 April 2023
Available online 26 April 2023

impact of climate change on the hydrological cycle in mountain regions, helping the maintenance of water resources quantity and quality, favouring their prolonged sustainable use.

The European Community proposed the Water Framework Directive 2000/60/EC and the Groundwater Directive 2006/118/EC to support the member countries in developing appropriate measures to guarantee the protection of groundwater resources from overexploitation and contamination. The first step of this process requires the definition of groundwater bodies that should represent the hydrogeological reference area to evaluate the availability and quality of groundwater resources. Generally, all the countries developed efficient 3D reconstructions of groundwater bodies of porous aquifers in the plain areas. However, the same is not valid for groundwater bodies in the mountain domain. Thornton et al. (2018) report that few 3D geological models exist in the Alps as a basis for interdisciplinary research and there is a general lack of scientific studies that identify groundwater bodies at a regional scale in mountainous environment (e.g., Arras et al., 2019). Studies on relatively small domains have been developed (e.g., Ballesteros et al., 2015; Turk et al., 2015) but their integration over larger domains is missing.

This study is focused on bridging the gap between local and regional studies by developing an approach for the identification of groundwater bodies in a complex Alpine area to cope with the requirements of European directives. The study area locates in Northern Italy and includes the mountain sector and part of the hilly sector of Lombardy Region (Fig. 1). In such area, more than 2.5 million inhabitants (ISTAT, 2021) live about 88% of annual withdrawals (371.4 million of cubic meters) derive from local groundwater for drinking purpose and other anthropic activities (ISTAT, 2019). First attempts in delineating groundwater

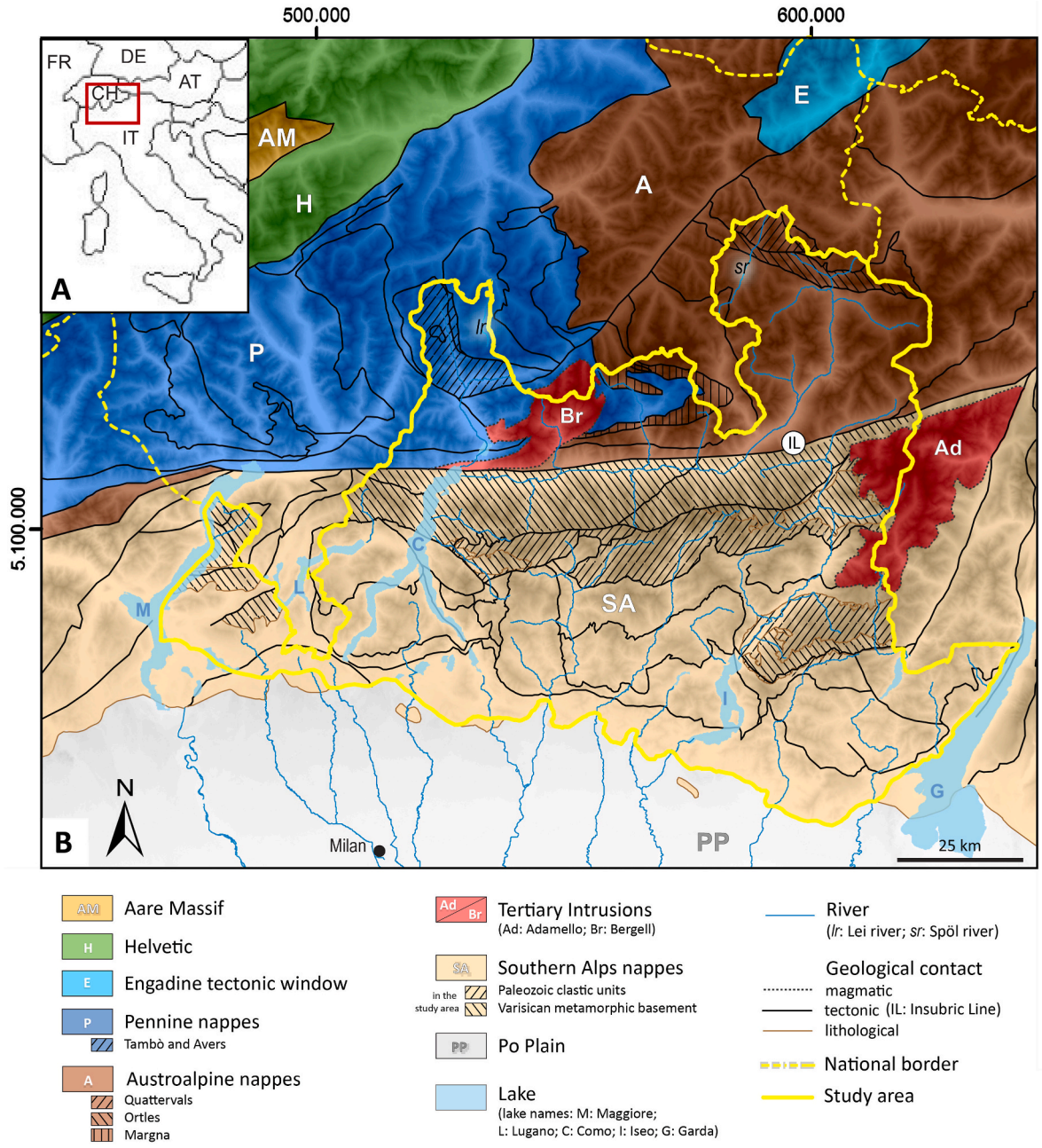

Fig. 1. The study area in the Central Alps of Italy. A) Location of panel B (red frame). FR: France; DE: Germany: CH: Switzerland; AT: Austria; IT: Italy. B) Structural sketch of the study area framed with the solid yellow line. (For interpretation of the references to colour in this figure legend, the reader is referred to the Web version of this article.)

bodies at national and regional levels and in estimating groundwater resources were done by Centro Lombardo di Studi ed Iniziative per lo Sviluppo Economico (1969), Commissione sulle risorse idriche in acque sotterranee dell'Italia (1982) and Beretta (1986). These studies were based on a 2D hydrogeological approach, through the definition of hydrogeological units, based on the hydraulic characteristics of the geological formations.

Sánchez et al. (2009) interpreted the guidelines for groundwater bodies identification (European Commission, 2003) suggesting two main criteria: i) the identification of hydrogeological boundaries and ii) the assessment of the quali-quantitative characteristics of the resource. In Alpine regions, the first criteria would lead to the identification of many bodies, theoretically one for each spring present in an area (i.e., more than three thousand for the case study). Apart from the scientific and technical difficulty to get to a reliable identification of such a large number of groundwater bodies, this approach does not allow the development of adequate policies at a regional level in terms of groundwater availability management, groundwater protection and groundwater monitoring. So, there is the need to define groundwater bodies that contain multiple single aquifers according to their nature (carbonate, porous, or fractured aquifers) and their chemical and quantitative status (second criteria of Sánchez et al., 2009). This integration is necessary to come to an efficient and sustainable groundwater management that allows to develop instruments and policies to face

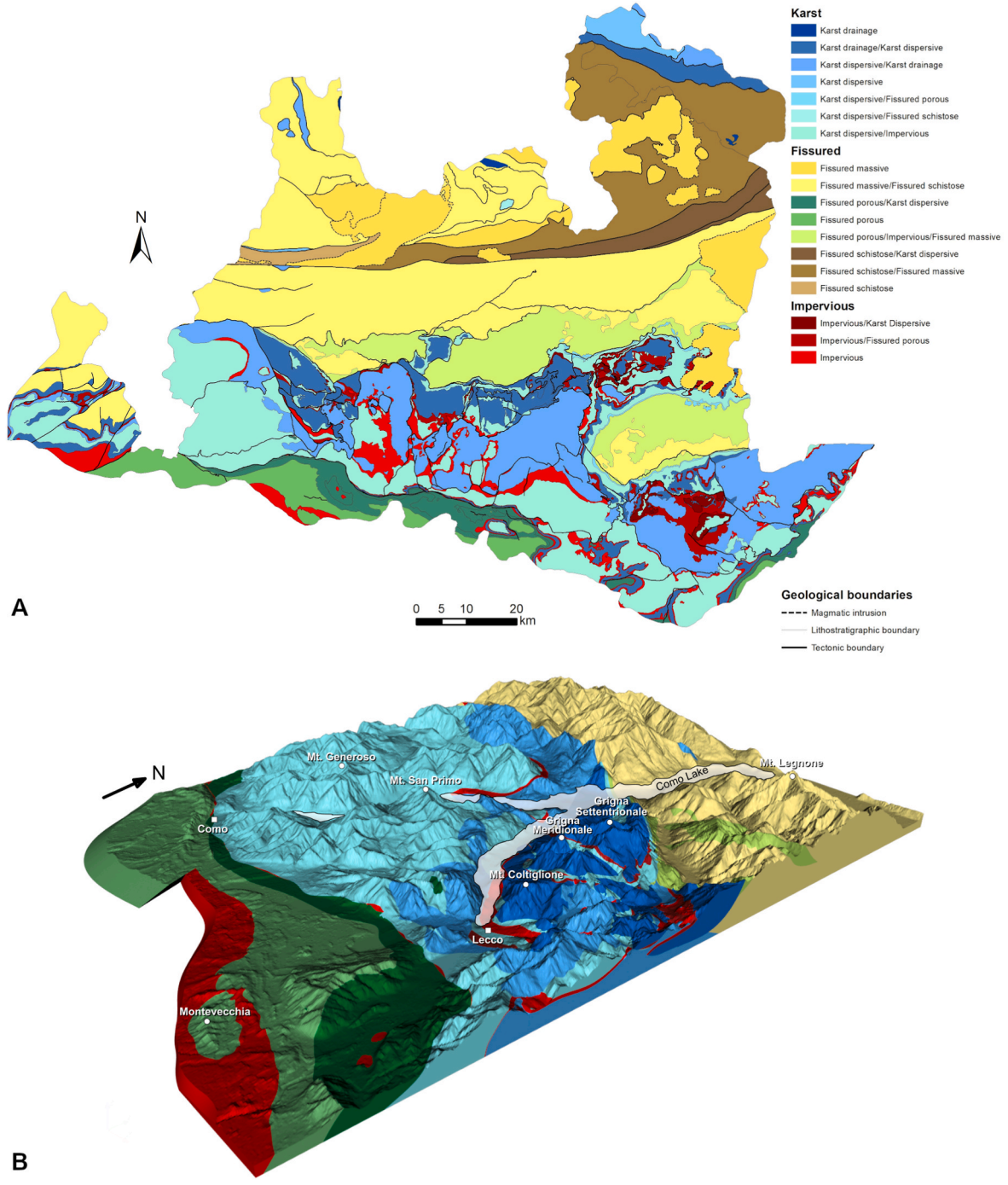

Fig. 2. Hydrostratigraphic model of the Alps of Lombardy after Masetti et al. (2022). A) Plan-view of the 3D model. B) 3D-view of the model sector around Como Lake. See Table 1 for the classification of the hydrostratigraphic units.

collective problems and needs, which are expected to vary as a result of changes of environmental and anthropogenic stressors.

On the basis of all these considerations, the main objectives of the study are: i) to identify and delineate groundwater bodies at a regional scale in a geologically complex Alpine environment according to European Directives; ii) to evaluate the distribution and quality of groundwater resources in the groundwater bodies and factors affecting them; iii) to identify areas of specific interest for supporting groundwater management (e.g., review of monitoring networks) and implementing groundwater policies (e.g., aquifer recharge areas protection).

The hydrogeological approach is supported by a 3D hydrostratigraphic study (Masetti et al., 2022) and makes extensive use of data collected and managed by the local public authorities (Environmental Regional Offices and Agencies).

2. Study area: geology and bedrock groundwater reservoirs of the Alpine mountains in Lombardy Region

2.1. Geological setting of bedrock aquifers

The study area covers a 10.290 km^2 wide sector of the Central Alps and of the southern foothills facing the Po plain in Lombardy Region, Northern Italy (Fig. 1-A). Almost all the surface waters of this area are collected by the tributaries of the Po basin, excluding the northernmost catchments of Lombardy (Lei and Spöl rivers, "lr" and "sr", respectively, in Fig. 1-B) that drain North, towards the Rhine and Danube basins. A North-dipping crustal fault, the Insubric Line ("IL" in Fig. 1-B), juxtaposes the stack of metamorphic nappes of the Central Alps to the North to the fold and thrust belt of the Southern Alps to the South (Fig. 1-B). It follows that two major geological and hydrostratigraphic domains characterise the mountains of Lombardy.

North of the Insubric Line, the Pennine and Austroalpine metamorphic nappes, intruded by the Bergell tonalite (Bigi et al., 1990; Br, Fig. 1-B), host groundwater bodies mostly into fissured crystalline rock-aquifers. Karst aquifers are rare. The largest ones occur at the North-eastern corner of the study area, represented by the Mesozoic carbonate rocks of the Ortles and Quattervals Upper Austroalpine nappe system (Fig. 1-B; Fig. 2; IHME, 1970; Deutloff et al., 1974; Mouton et al., 1982; Bigi et al., 1990). A few small-sized and isolated metamorphic carbonate masses occur westwards, belonging to the metasedimentary cover of the Austroalpine Margna nappe and Pennine Tambò and Avers nappes (Fig. 1-B; Fig. 2).

South of the Insubric Line the Southern Alps are characterised by a South-verging thick-skinned fold and thrust belt intruded by the Cenozoic Adamello batolith (Ad, Fig. 1-B). In detail, the South-verging belt involves a Variscan metamorphic basement with Paleozoic clastic tegument and the decoupled Meso-Cenozoic sedimentary cover units, which are mostly carbonates. In the Southalpine belt, karst aquifers occupy about 60% of the total area, representing the largest and most productive groundwater reservoirs of Lombardy Region. Metamorphic basement rocks and the Adamello intrusive masses mainly host fissured aquifers, while the Permian and Cretaceous-Cenozoic clastic sediments mainly behave like fissured aquifers with some inter-granular porosity.

2.2. 3D hydrostratigraphic/hydrostructural model

The conceptual model and the 3D architectural model of the region are presented in Masetti et al. (2022). Fig. 2 shows the hydrostratigraphic map derived from the plan-view of the 3D model; Table 1 provides the definition of the adopted hydrostratigraphic categories.

The 3D hydrostratigraphic/hydrostructural model described in Masetti et al. (2022) applied the current classification criteria for hydrogeological mapping (Struckmeyer and Margat, 1995; Günther and Duscher, 2019) to the bedrock units as defined in the regional geology literature, respecting the geometry of their boundaries. The model describes the lithological, geometrical, and geomorphological components

Table 1
Hydrostratigraphic classification adopted for bedrock aquifers of the Alps of Lombardy (after Masetti et al., 2022). The dominant flow classes are listed from top to bottom in the expected descending order of hydraulic conductivity.

Dominant flow characteristics	Dominant flow classes	Definition
KARST	**Karst drainage**	Carbonate karst rock units with large and extensively connected conduits and caves: massive and thick-bedded limestones, dolostones and marbles
	Karst drainage/Karst dispersive	Lateral and vertical association of Karst drainage prevailing over Karst dispersive rocks
	Karst dispersive/ Karst drainage	Lateral and vertical association of Karst dispersive prevailing over Karst drainage rocks
	Karst dispersive	Carbonate rock units with network of small-scale karstified fractures and bedding planes with few or no major conduits and caves
	Karst dispersive/ Fissured porous	Lateral and vertical association of Karst dispersive (massive dolostones, vacuolar dolomitic limestones) prevailing over Fissured porous rocks (breccias, siltstones).
	Karst dispersive/ Fissured schistose	Lateral and vertical association of Karst dispersive prevailing over Fissured schistose rocks: folded and transposed marble lenses and ophicarbonates with schists
	Karst dispersive/ Impervious	Lateral and vertical association of Karst dispersive rocks prevailing over Impervious rocks: limestone and dolostone/marlstone and shale alternances.
FISSURED	**Fissured massive**	Isotropic to poorly anisotropic fissured rock units: intrusive, effusive and pyroclastic bodies; poorly foliated metamorphic units
	Fissured massive/ Fissured schistose	Folded association of Fissured massive (intrusive masses, orthogneisses, paragneisses, quartzites) prevailing over Fissured schistose rocks (micaschists, slates, shales)
	Fissured porous/ Karst dispersive	Lateral and vertical association of Fissured porous (clastic) prevailing over Karst dispersive rocks (bedded limestones)
	Fissured porous	Massive to bedded, fissured clastic rocks with some intergranular porosity: conglomerates, breccias, sandstones, siltstones with subordinate shale interbeddings
	Fissured porous/ Impervious/Fissured massive	Lateral and vertical association of Fissured porous rocks (conglomerates, breccias, sandstones, siltstones), prevailing over Impervious (shales) and Fissured massive rocks (ignimbrites and tuffs)
	Fissured schistose/ Karst dispersive	Lateral and vertical association of Fissured schistose prevailing over Karst dispersive rocks: tightly transposed schists and foliated metamorphites with marbles
	Fissured schistose/ Fissured massive	Folded association of Fissured schistose (micaschists, paragneisses, phyllites, slates, shales) prevailing over Fissured massive (intrusive masses, orthogneisses, quartzites)
	Fissured schistose	Strongly anisotropic, foliated, poorly or locally fissured rock units (paragneisses, micaschists, shales, slates)

(*continued on next page*)

Table 1 (*continued*)

Dominant flow characteristics	Dominant flow classes	Definition
IMPERVIOUS	Impervious/Karst dispersive	Association of Impervious rocks prevailing over Karst dispersive: shale-carbonate alternances
	Impervious/Fissured porous	Association of Impervious rocks (shales) prevailing over Fissured porous rocks (sandstones and siltstones)
	Impervious	Isotropic to anisotropic fine-grained, poorly fractured, practically non-aquifer rock units: shales, mudstones, marlstones

of the geological heterogeneity, accounting for the dominant groundwater circulation patterns through the geological units that compose the bedrock water reservoirs (Table 1; Fig. 2).

i) Lithological component of heterogeneity.

Groundwater flow in the Alpine bedrock of Lombardy predominantly occurs through karst and fissured rocks. Intergranular porosity represents a subordinate flow-path, mostly occurring in fissured clastic rocks. Besides, the hydraulic properties of Alpine rocks depend on the existing anisotropies too. These are mainly represented by bedding planes and foliations *l.s.* (labelled as "schistose"). In their absence, the rock units are considered as dominantly isotropic (i.e., "massive").

The hydraulic conductivity of karst aquifers characterised by large, extensive, and well-connected caves and conduits markedly differs from the conductivity of carbonate units where only a diffuse network of minor, small-scale conduits and karstified fractures and bedding planes occur (Sauter et al., 2008; Vigna and Banzato, 2015; Medici et al., 2021). In this study, the first type of karst aquifer is named "karst drainage", while the second "karst dispersive".

The least permeable, practically non-aquifer rocks, like shales, marlstones, and mudstones, are considered as "impervious" and form the aquitards and aquicludes.

The resulting classification adopted for the bedrock aquifers of the Lombardy Alps shown in Table 1 was obtained considering the spatial variations of these characteristics through the geological units modelled in 3D and the distribution and average discharge (0–0.8 $m^3 s^{-1}$) of the known springs (n. 3443) in the study area. The classification scheme consists of eighteen classes obtained by combining the dominant groundwater flow characteristics (karst, fissured, impervious) with the subordinate concurrent properties (intergranular porosity, anisotropy vs. isotropy) and accounting for the vertical and/or lateral associations of different flow classes within the modelled geological units (in this latter case a "/" connects the classes to generate the corresponding term).

ii) Geometrical component of heterogeneity.

At the regional scale it is represented by the 3D modelled geometry of the geological units (Fig. 2). It derives from the combination of the primary external geometry of sedimentary and magmatic bodies with the secondary (tectonic) deformation patterns of the sedimentary, magmatic, and metamorphic basement units (superimposed fold, thrust and fault systems).

iii) Geomorphological component of heterogeneity.

It is mirrored by the present-day topography that represents one of the boundaries of the aquifer rock volumes. It also contributes to determine the presence of subsurface groundwater divides by the combination of topographic effects and subsurface heterogeneity (Welch and Allen, 2014) and exposing impervious units. A 30 m × 30 m DTM was used at this purpose (JAXA, 2021).

The 3D geomodelling of the heterogeneity components led to identify and represent the boundaries of the regional-scale elements of the hydrostratigraphic architecture, which is the starting point to identify the groundwater bodies. Three different types of geological surfaces were modelled, which might correspond to volumetric boundaries of aquifer units.

a) boundaries of lithostratigraphic confining layers, which are aquitard/aquiclude hydrostratigraphic units (Table 1; Fig. 2). These boundaries are the expression of the lithological and primary geometrical components of heterogeneity;
b) tectonic boundaries, which might act as aquitard/aquicludes when determining a continuous vertical or lateral juxtaposition of aquifers against aquitard/aquiclude units. Tectonic boundaries are the expression of the tectonic component of heterogeneity and may be represented by thrust-faults, nappe contacts or high-angle faults, that *per se* could be either permeable or impermeable (see discussion and references in Medici et al., 2021). The possible confining effect recognised at the regional scale is mostly determined by the lithological contrasts along the boundary, related to the pattern of groundwater circulation within the juxtaposed rock volumes;
c) geomorphological boundaries, which are erosional surfaces that cause intersections between the present-day topographic surface and the laterally persistent aquitard/aquiclude units, determining the presence of springs along the valley slopes.

The presented 3D model constitutes the base for the identification and characterisation of the groundwater bodies in the study area. Details, including an example of 3D model inspection, are given in Sections 3 and 4.

3. Materials and methods

Section 3 describes the materials and methodologies used in this study. Section 3.1 describes the materials used for the calculation of the groundwater budget, in terms of processed data and their original source, spatial and temporal resolution, and the methodologies applied for the calculation of the budget on an annual basis and discretising the studied domain on a grid basis. Section 3.2 describes the hydrochemical and isotopic dataset and the analyses performed for the characterisation of groundwater chemistry and the identification of spring recharge areas. Section 3.3 describes the criteria adopted for the identification and delineation of groundwater bodies through the inspection of the 3D hydrostratigraphic model (Masetti et al., 2022) and the evaluation of: i) their consistency with previous local and regional studies, ii) the agreement of hydrochemical data of groundwater with the lithological characteristics within each groundwater body, iii) the uncertainty in groundwater budget.

3.1. Groundwater budget terms

The groundwater budget was computed for evaluating the availability and distribution of groundwater resources within the identified groundwater bodies. The budget was evaluated on an annual basis and included the following terms and data.

1) monthly and annual cumulative precipitation, as average of data collected in the period 2014–2018 (Table 2, a-b);
2) monthly and annual cumulative snowmelt, as a result of weekly snow water equivalent (SWE) data, obtained through the combination of cumulative weekly snow heights (Table 2, c-d), maximum weekly snow coverage (Table 2, e) and snow density (literature data);

Table 2
Data used for the evaluation of the groundwater budget. Acronyms: ARPA Lombardia (Regional Environmental Agency – Lombardy Region), Italy; MeteoSWISS (Federal Office for Meteorology and Climatology), Switzerland; c) NASA (National Aeronautics and Space Administration), MODIS (Moderate Resolution Imaging Spectroradiometer), U.S.A.

Id	Data	Source	Spatial resolution	Temporal resolution	Source link
a	Cumulative precipitation	ARPA Lombardia	n. 130 meteorological stations	daily data, 2014–2018	https://www.arpalombardia.it/
b	Cumulative precipitation	MeteoSWISS	n. 23 meteorological stations	daily data, 2014–2018	https://www.meteoswiss.admin.ch/
c	Cumulative snow height	ARPA Lombardia	n. 29 meteorological stations	daily data, 2014–2018	https://www.arpalombardia.it/
d	Cumulative snow height	MeteoSWISS	n. 12 meteorological stations	daily data, 2014–2018	https://www.meteoswiss.admin.ch/
e	Maximum extension of snow cover (SCA)	NASA, MODIS/Terra Snow Cover 8-Day L3 Global 500 m SIN Grid, Version 6	500 m (at nadir)	8-days window data, 2014–2018	https://earthdata.nasa.gov/earth-observation-data/near-real-time/download-nrt-data/modis-nrt
f	Mean air temperature	ARPA Lombardia	n. 118 meteorological stations	daily data, 2014–2018	https://www.arpalombardia.it/
g	Mean air temperature	MeteoSWISS	n. 23 meteorological stations	daily data, 2014–2018	https://www.meteoswiss.admin.ch/
h	Streamflow discharge	Regional Water Budget, Lombardy Region and ARPA Lombardia (Regione Lombardia, 2016)		2001–2015	https://idro.arpalombardia.it/manual/bilancio_idrico.html
i	Licenced withdrawals from springs (average values)	Cadastre, Lombardy Region	n. 3443 springs	–	Data available upon request

3) annual evapotranspiration obtained from precipitation, snowmelt and air temperature data, through the application of the formula proposed by Turc (1954); monthly average air temperature was calculated from data collected in the period 2014–2018 (Table 2, f-g);
4) streamflow discharge of each watershed, obtained from the evaluation of an inflow-outflow model applied at a regional scale, calibrated on streamflow discharge measured at gauging stations (Table 2, h);
5) groundwater flow discharge, expressed as the volume per unit time of withdrawals from the springs declared to the competent regional authorities and licenced (Tables 2 and i).

The groundwater budget symbolic equation adopted in this study is presented below:

$$(P - ET) = (SW + GW) + \varepsilon \quad \text{Eq. 1}$$

where P is the precipitation amount, including the rainfall and the snowmelt terms; ET is the evapotranspiration component; SW is the streamflow discharge of each watershed; GW is the sum of agricultural, industrial, sanitation-hygienic, and drinking declared and licenced withdrawals from springs; ε represents the uncertainty term including the systemic error in the evaluation of the variables and the surplus/deficit amount in (ground)water resources. The potential contribution of glacier and rock glacier melting is neglected because: i) despite recent studies have shown an average glacier area loss of −14% in the Alpine area in the period 2003–2015/2017 (e.g., Paul et al., 2020), it was not possible to estimate from literature the amount of water deriving from the glacier melting annually and potentially contributing to the groundwater budget in the study area as inflow or outflow terms; ii) despite the numerousness of rock glaciers and protalus ramparts in the study area (Scotti et al., 2013) and their non-negligible water storage function on a long-term period, few studies propose reliable methods to estimate their contribution to surface and groundwater flows (Jones et al., 2019); iii) previous studies related to surface water flow, whose data are assimilated in this work, did not consider this term (Regione Lombardia, 2016).

The budget terms were discretised according to a regular squared grid, with cell dimensions of 300 m × 300 m, in the WGS 84 - UTM zone 32 Nord projection. Measurement units of each budget term were expressed as annual volume per unit area: $[L^3]/[T] \times [L^2]$. The budget terms were prepared through the combined use of programming languages (Matlab, Mathworks® and R, https://www.r-project.org/) and geographical information systems (ArcGIS, ESRI®). The pre-processing of the ground-based data (rainfall, temperature, snow height) and the preparation of geographical variables to be used for the spatial interpolation of ground-based data were performed in Matlab (Mathworks®) and ArcGIS (ESRI®) environments, respectively. The spatial interpolation of ground-based data was performed in R environment. The processing of the snowmelt variable, the preparation of the variables representing the surface- and groundwater flow terms and the calculation of the groundwater budget terms for each groundwater body were performed in ArcGIS (ESRI®).

3.1.1. Interpolation of ground-based data: precipitation, snow height and air temperature

The spatial distributions of precipitation, air temperature and snow height were obtained interpolating daily measurements, retrieved from the Italian and Swiss meteorological networks located in the mountainous and plain areas within or in close proximity of the study area (Fig. 1; Table S1 in the Supplementary Material). These meteorological stations were selected for the completeness of data in the 2014–2018 period and to reduce the interpolation uncertainties along the borders of the study area. Different regression models and interpolation techniques were tested and evaluated, both singularly and combined. The combination methods apply a regression model, followed by the interpolation of the residuals and the subsequent summation of the two contributions. This methodology allows the selection of geographical variables for regression, focusing the attention on the physical processes and on the climatology that dominates the precipitation events over the study area (Camera et al., 2014; Sekulić et al., 2020). The comparison of several regression models and interpolation techniques allows identifying the most appropriate method to be used in the construction of the gridded climate data for the case study (Hofstra et al., 2008).

The selected simple interpolation and regression techniques were: geographically weighted regression (GWR), inverse distance weighting (IDW), linear multiple regression (LMR) and 3D thin plate sp-lines (TPS). These 4 techniques were combined as follows: GWR + IDW, GWR + TPS, LMR + IDW, LMR + TPS. Totally, eight interpolation and regression

techniques were tested. Refer to Camera et al. (2014) for a complete description of regression models and interpolation techniques and correspondent R libraries. The selected geographical variables for the interpolation of precipitation and air temperature were: elevation, North coordinate, East coordinate, slope. The geographical variables selected for the interpolation of snow height were: elevation, aspect, slope, North coordinate, concavity/convexity.

For the purposes of the water budget calculation, daily data of precipitation and air temperature were aggregated on a monthly basis. In case of missing values exceeding 10% in a specific month, the monthly value was not calculated, and a missing value assigned. Subsequently, for each month of the 2014–2018 period, the average value of the variable was calculated, ignoring possible missing values.

The interpolation of snow height values was performed considering the maximum snow height measured at the stations during the eight-day window of acquisition of the snow cover extension. This choice assumes that the maximum snow height corresponds to the maximum snow cover area. In case of 80% or more of the stations with zero or missing data, the interpolation of snow height data was not performed. Therefore, the interpolation of snow height data was not performed for the months from June to October.

The different interpolation and regression techniques were evaluated through four skill scores and leave-one-out validation. The selected set of indices contains both absolute error and goodness-of-fit measures, as suggested by Legates and McCabe (1999). The four skill scores are: Nash-Sutcliffe coefficient (NSE; Nash and Sutcliffe, 1970), Kling-Gupta coefficient (KGE; Kling et al., 2012), percent bias (PBIAS) and mean absolute error (MAE). The scores were evaluated through the R-library *hydroGOF* (https://cran.r-project.org/web/packages/hydroGOF/hydroGOF.pdf). The technique showing the best balance between overall performance and simplicity of computation was used in the following budget calculations.

3.1.2. Combination of ground-based and remote sensing data for the snow related term

The snowmelt term for the winter - spring period from November to July was obtained applying the classical equation (Seibert et al., 2015) that converts snow height data (H_s) into Snow Water Equivalent (SWE):

$$SWE = H_s \frac{\rho_{snow}}{\rho_{water}} \quad \text{Eq. 2}$$

where ρ_{snow} is snow density, and ρ_{water} is water density. SWE is expressed in the same unit measure of H_s [L]. An average snow density value equal to 150 kg m^{-3} was attributed based on literature about snow properties in the Italian Alps (Guyennon et al., 2019; Valt et al., 2018). Water density was set at the commonly used 1000 kg m^{-3} value.

Then, SWE was related to the maximum snow cover area (SCA) in the same eight-day window of satellite acquisition, as a product between the two datasets. This methodology was successfully applied in regional studies in mountainous areas (e.g., Filippa et al., 2019). The maximum SCA was obtained from MOD10A2 data (Hall and Riggs, 2016) by transforming the original dataset in a binary mask representing "snow" (1) vs. "no snow" (0) areas, according to Table S2 in the Supplementary Material. It was decided to consider "lake ice" as "snow" because during winter, in high elevation areas, lakes were alternatively mapped as "snow" or "lake ice", leading to a misinterpretation of the presence or absence of snow and causing not justifiable variations of snow height. Thus, also considering the ratio between the grid (0.25 km^2) and the Alpine lakes (2.0 km^2) extensions, we reclassified "lake ice" cells into "snow" cells. "Clouds" cells were reclassified as "snow" cells because the obstruction due to the presence of clouds did not allow to discriminate between snow presence/absence. Thus, we assumed that the snow height dataset obtained through the interpolation of ground-based data was the best evaluation.

The monthly snowmelt term was obtained by adding the weekly (i.e., eight-day) snowmelt terms related to the same month. Then, for each month of the period November–July between 2014 and 2018, the average monthly snowmelt was calculated, by applying the following corrections.

a) to consider the occurrence of compaction and melting processes during December, January and February, a filter related to the elevation was applied: melting was not calculated for areas located at an elevation higher than 2000 m a.s.l. (i.e., at these elevations, during the specified months, a reduction of snow height was interpreted as compaction);
b) to evaluate the melting process occurring in June and July, overcoming the lack of ground-based data allowing a reliable interpolation of snow height data, a filter related to the elevation was applied through the following formulas:
    - o monthly melting in June is equal to the available (on ground) SWE calculated over the last week of May (i.e., day 145 to day 152) for areas at an elevation equal to or lower than 3000 m a.s.l., whereas it is equal to the half of the SWE calculated for the last week of May for areas located at an elevation higher than 3000 m a.s.l.;
    - o monthly melting in July is equal to the half of the SWE calculated over the last week of May for areas located at an elevation higher than 3000 m a.s.l., whereas it is zero for areas at an elevation equal to or lower than 3000 m a.s.l., where everything melted in June.

3.1.3. Calculation of the evapotranspiration term

Among the various methods for estimating evapotranspiration (e.g., Lu et al., 2005; McKenney and Rosenberg, 1993), we selected Turc's formula (1954), which uses precipitation amount and air temperature as inputs. The reliability of this method is confirmed by studies in European areas both at a regional (e.g., Parajka and Szolgay, 1998; Horvat and Rubinic, 2006; Allocca et al., 2014) and a local scale (e.g., Havril et al., 2018). We applied Turc's formula as follows:

$$ET = \frac{P}{\sqrt{\left(0.9 + \frac{P^2}{L^2}\right)}} \quad \text{Eq. 3}$$

where ET is the annual evapotranspiration (mm y^{-1}), P is the annual cumulative precipitation (mm), which comprises both rainfall and snowmelt in this study, L is the evaporative potential of the atmosphere, calculated as:

$$L = 300 + 25 \bullet Tc + 0.05 \bullet Tc^3 \quad \text{Eq. 4}$$

where Tc is the annual average diurnal temperature (°C) modified according to the amount of precipitation (Civita, 2005), calculated as:

$$Tc = \frac{\sum_{i=1}^{12} T_i \bullet P_i}{\sum_{i=1}^{12} P_i} \quad \text{Eq. 5}$$

being P_i and T_i the monthly cumulative precipitation and the monthly average daily temperature, respectively.

3.1.4. Surface- and groundwater related terms

Streamflow discharge for each watershed was extracted from the Regional Water Budget (Table 2; Regione Lombardia, 2016). At the outlet of each watershed, the Regional Water Budget reports the modelled streamflow discharge related to the entire upstream catchments, referred to the period 2001–2015 and expressed in $m^3\ s^{-1}$. The streamflow discharge is modelled through RIBASIM (RIver BAsin SIMulation; Deltares) and calibrated with discharge measurements at specific gauging stations. Watershed properties are provided as a vectorial (polygonal) dataset. In this study the net discharge produced

within each (sub-)watershed is needed. Thus, streamflow discharges of each watershed were recalculated by subtracting the discharges flowing in from watersheds located upstream (if present). Then, the vectorial dataset was transformed in a raster dataset, where each cell contains the streamflow discharge value divided by the watershed extension, so to express the term as annual volume of water ($m^3\ y^{-1}$) per unit area (m^2).

The groundwater related term is represented by withdrawals from springs managed by public and private water users for industrial, agricultural, sanitation-hygienic, and drinking purposes. Lombardy Region manages the licenses for the usage of groundwater for these purposes, and collects data referred to each spring or group of springs in a cadastre (Table 2). As withdrawals are not related to a defined catchment, the withdrawals for each spring or group of springs were expressed as annual volume of water ($m^3\ y^{-1}$) to be used in the water budget calculation.

3.2. Hydrochemical features

The hydrochemical characteristics of groundwater in the Lombardy Region are monitored by the Regional Environmental Agency (ARPA Lombardia) with a six-month frequency. The hydrochemical dataset provided for the Alpine mountainous area includes data from 65 springs used for drinking purposes and covers the period 2014–2018. The database includes spring coordinates and elevation, main physico-chemical parameters (temperature, electrical conductivity, pH), major anions and cations, minor elements (e.g., metals) and contaminants (e.g., solvents, pesticides). The average value of each parameter was calculated for characterising each monitoring point; non-detectable values were set equal to the limit of detection. Moreover, 31 of the 65 springs were selected to perform the analysis of the water stable isotopes component (δ^2H and $\delta^{18}O$). Water samples were collected in August–September 2021.

A series of descriptors, diagrams, bivariate plots, and spatial distributions were evaluated to perform the characterisation of groundwater chemistry.

a) descriptive statistics for chemical elements and compounds concentrations, EC, pH and temperature values: arithmetic mean, median, minimum and maximum values and standard deviation;
b) Piper Diagram in its color-coded modification (Piper, 1944; Peeters, 2014), and Schoeller Diagram (Schoeller, 1962) for the identification of hydrochemical facies;
c) comparison between average water temperature and its variation in the monitoring period 2014–2018 (±2 °C) for recognising the groundwater flow circulation (deep or shallow circulation) and features related to it;
d) spatial distribution of electrical conductivity, pH, calcium/magnesium ratio, sulphates, nitrates, metals (i.e., arsenic, iron, zinc) for recognising local geological features for groundwater circulation;
e) bivariate plots of major and minor compounds to identify water-rock interaction processes and potential anthropogenic contaminations;
f) δ^2H - $\delta^{18}O$ plot and $\delta^{18}O$ - elevation to obtain information on groundwater origin and recharge areas of the groundwater circulation systems.

3.3. Identification of groundwater bodies

Groundwater bodies are here defined as rock entities containing aquifers and/or aquitards/aquicludes independent from the aquifers located in adjacent or upper/lower rock entities, according to water recharge, groundwater circulation, and hydrochemical characteristics. This definition is similar to the concept of "Aquifer Group" according to Maxey (1964) and Domenico and Schwartz (1990) for porous aquifers and follows the approach of Sánchez et al. (2009) described in the Introduction Section.

Groundwater bodies were identified through the inspection of the 3D hydrostratigraphic model (Masetti et al., 2022, Fig. 2-B) combined with the location of springs and checking their relationship with the location and geometry of the boundary elements. This phase required the comparison with regional and local studies on groundwater circulation and hydrochemical characteristics. In particular, the delineation of groundwater bodies had to satisfy: i) the tracer test results conducted on groundwater flow in karstic areas (Tognini et al., 2011; Ferrario and Tognini, 2016); ii) the known limits of the hydrogeological catchment of specific springs (e.g., Citrini et al., 2021); iii) the relationship between the physico-chemical characteristics of a spring and its recharge area (e.g., Ciancetti and Pilla, 2001; Gambillara et al., 2013; Volpi et al., 2017); iv) the coherence between the recharge area of a spring and the range of elevation recharge derived from the isotopic signature of groundwater (Longinelli and Selmo, 2003; Citrini et al., 2021). In addition, a critical review of the results of the groundwater budget was carried out to identify and evaluate the uncertainties related to the delineation of groundwater bodies. A case-by-case analysis was performed comparing inflow and outflow terms of the groundwater budget for each groundwater body. Inflow and outflow terms, for each groundwater body, were calculated summing the contribution of all the cells (300 m × 300 m) included in each one of them.

4. Results

4.1. Groundwater budget calculation

The performance evaluation of the interpolation techniques used for ground-based data is shown in Table 3. The selected interpolator for monthly cumulative rainfall and average air temperature is the 3D thin plate sp-lines (TPS). Instead, the best interpolator for weekly snow heights is the combination of linear multiple regression and 3D thin plate sp-lines (LMR + TPS).

A spatial representation of the groundwater budget terms is shown in Fig. S1 in the Supplementary Material. Annual cumulative rainfall ranges between 720 mm and 1950 mm, with the highest values occurring in the mountain ridge located in the middle of the study area, approximately in correspondence of the Variscan metamorphic basement of the Southern Alps Nappes between the Como Lake and the Adamello Pluton (Fig. 1), and the lowest values in the north-eastern and south-eastern corners of the study area, near the Swiss border and Lake Garda, respectively. The spatial distribution of rainfall values is coherent with previous studies conducted at a regional and national scale over

Table 3
Summary of the performance evaluation of the eight interpolation and regression techniques (see 3.1.1) for rainfall, air temperature and snow heights. Skill scores: Nash-Sutcliffe coefficient (NSE), Kling-Gupta coefficient (KGE), percent bias (PBIAS) and mean absolute error (MAE).

Method	NSE	KGE	PBIAS	MAE
Rainfall				
IDW	0.47	0.59	0.03	18.78
TPS	0.53	0.64	−0.07	17.06
LMR + IDW	0.44	0.59	0.49	19.83
Air temperature				
IDW	0.56	0.70	−3.20	2.15
TPS	0.95	0.97	−0.34	0.63
GWR + IDW	0.95	0.96	2.24	0.65
LMR + IDW	0.95	0.95	2.01	0.68
LMR + TPS	0.96	0.97	−0.08	0.60
Snow heights				
LMR	0.23	0.48	−1.11	44.16
LMR + IDW	0.26	0.50	−4.47	41.29
LMR + TPS	0.35	0.63	−0.31	39.31
GWR	0.25	0.51	0.32	43.03
GWR + IDW	0.28	0.54	−3.69	40.69
GWR + TPS	0.34	0.62	0.41	39.73

different periods of time (1891–1990, Ceriani and Carelli, 2003, 1961–1990, Crespi et al., 2018, 1800–2016, Crespi et al., 2021, 2001–2015, ARPA Lombardia, www.arcis.it). Due to the occurrence of snowmelt, annual cumulative precipitation amounts increase, ranging between 800 mm and 2780 mm and reflecting the same spatial distribution of the sole rainfall amount.

Evapotranspiration values range between 170 and 760 mm y^{-1}. As expected, the highest values occur in the southern part of the study area, close to the plain. Whereas the lowest values correspond to the highest mountainous ridges and peaks, located close to the border with Switzerland (northern side) and Trentino-Alto Adige Region (north-eastern side).

According to the Regional Water Budget (Regione Lombardia, 2016), 409 catchments are totally or partially included within the study area. The mean and median streamflow discharges normalised according to the extension of each catchment are equal to 1.04 and 0.98 $m^3 y^{-1} m^{-2}$. Outliers (19 out of 409) represent anomalies in the distribution of the net discharge produced within each (sub-)watershed along the network. In two cases, one (sub-)watershed shows a normalised discharge value much lower (i.e., showing an extremely low outlier value) respect to the upstream (sub-)watershed it is connected with (i.e., showing an extremely high outlier value). This fact could be due to an under- or overestimation of the variables considered in the inflow-outflow model. Nonetheless, for the purpose of the groundwater budget calculation, further corrections of discharge data were not applied.

The total groundwater withdrawal derived from the 3443 springs

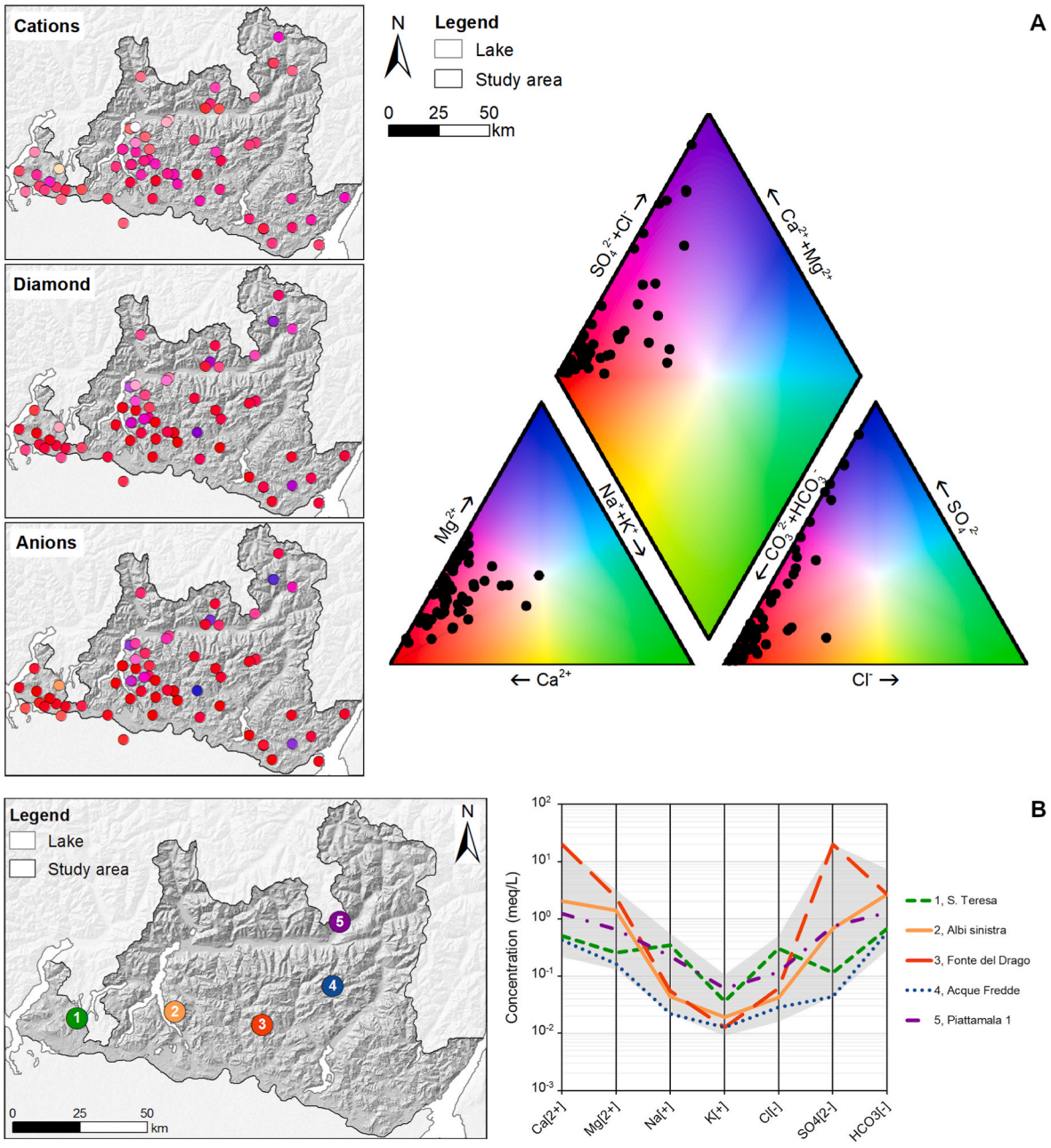

Fig. 3. A) Color-coded Piper plot modified after Peeters (2014) with corresponding color-coded maps. B) Location of five selected springs and Schoeller diagram: the grey shadow shows the range of variation of the 7 compounds for the 65 springs; the coloured lines represent the chemical composition of 5 springs selected as characteristics of the study area: 1, S. Teresa (Cuasso al Monte); 2, Albi sinistra (Mandello del Lario); 3, Fonte del Drago (Oltre il Colle); 4, Acque fredde (Vilminore di Scalve); 5, Piattamala 1 (Tirano). Right: location of the selected springs. Basemap: hillshade; source: https://osm-wms.de/(For interpretation of the references to colour in this figure legend, the reader is referred to the Web version of this article.)

registered in the regional cadastre is equal to 13.88 $m^3\ s^{-1}$, which is equivalent to about 438 × $10^6\ m^3\ y^{-1}$. About 55% of the springs show a withdrawn discharge equal to or lower than 0.001 $m^3\ s^{-1}$, the 37% shows a withdrawn discharge ranging between 0.001 $m^3\ s^{-1}$ and 0.1 $m^3\ s^{-1}$, and the 8% shows a withdrawn discharge higher than 0.1 $m^3\ s^{-1}$. Springs showing the highest discharges are located in the southern part of the study area, in correspondence of the most productive aquifers (carbonate formations) and the most populous urban areas (Bergamo, Brescia and Varese administrative provinces; Fig. S2 in the Supplementary Material; ISTAT, 2021).

4.2. Hydrochemical characterisation

The Ca–HCO_3 type is the prevalent hydrochemical facies in the study area, followed by the Ca–SO_4 type (Fig. 3-A). From the Piper diagram, the cations cluster around high Ca^{2+} percentages, with Mg^{2+} percentages lower than 50% and few samples do not present any dominant cation. The anions cluster along a line between CO_3^{2-}+HCO_3^- and SO_4^{2-} dominant facies, with low percentages of Cl^-. Such results are partially biased by the major number of springs located in the carbonate formations (i.e., the most productive aquifers), respect to those located in clastic formations and magmatic/metamorphic units. The Piper Diagram in its color-coded modification by Peeters (2014) is based on the Hue, Saturation and Value (HSV) color scheme. By assigning these colours to the sampling locations on maps, a direct link between the sampling location, the lithology, the geological structure and the Piper plot is established to facilitate the interpretation of hydrochemical data (Fig. 3-A). Differences in hydrochemical compositions are marked by the transition from red-purple colours to the pink-violet colours in the diamond plot and map, highlighting slight-to-moderate differences among springs located very close to each other. Other differences in compositions are highlighted in the cation (pink to white colours) and anion (violet to blue colours) maps: the first highlighting alkaline compositions of spring waters, the second highlighting sulphate compositions.

Fig. 3-B shows the general variability of the hydrochemical compounds of spring waters in the study area. In general, the Schoeller diagram confirms the prevalence of Ca^{2+} and HCO_3^-, whereas Na^+, K^+ and Cl^- are present in low concentrations. Nonetheless, exceptions within the general hydrochemical composition reflect the geological variability of the Lombardy Alpine territory. Five springs are selected as representative of the different hydrochemical facies (Fig. 3-B).

- Piattamala 1 (Tirano). The spring is located in the Austroalpine metamorphic basement, here constituted by micaschists. Spring water show ion concentrations similar to the average trend, but higher values of Na^+ and K^+.
- S. Teresa (Cuasso al Monte). The spring is located in correspondence of the Southalpine metamorphic basement. Ca^{2+}, Mg^{2+} and HCO_3^- concentrations are lower than the average trend, but with Na^+ and Cl^-concentrations higher than the average trend.
- Albi sinistra (Mandello del Lario). The spring is located in the Triassic carbonates of the Southalpine cover, in particular in correspondence of the contact between limestone-dolostone and limestone-marl formations. The trend of the compositional line in the Schoeller diagram reflects the general trend of all the springs, with high concentrations of Ca^{2+} and HCO_3^- and higher concentrations of Mg^{2+} respect to the average trend, reflecting the circulation in limestone-dolostone or dolostone rocks.
- Fonte del Drago (Oltre il Colle). The spring is located in correspondence of a Southalpine thrust that separates massive limestones and dolostones (carbonate platform deposits) from arenite and limestone-claystone basin lithofacies, with local evaporite lenses. The hydrochemical facies of the spring water with high concentrations of Ca^{2+} and SO_4^{2-}, reflects circulation through the observed carbonate and claystone-evaporite rocks, respectively.
- Acque Fredde (Vilminore di Scalve). The spring is located in the Southalpine Permian clastic formations. Compound concentrations are among the lowest ones measured in the samples, with minimum values of Na^+ and SO_4^{2-}.

In general, groundwater quality is very high, being suitable for drinking purposes. None of the springs show detectable concentrations of hydrocarbons (i.e., aromatic hydrocarbons), chlorinated solvents or pesticides (ARPA Lombardia, https://www.arpalombardia.it/Pages/RSA/Acque.aspx). Metals are not detected in groundwater as well, with some exceptions for As, Fe and Zn. During the monitoring period, the physico-chemical and hydrochemical parameters do not exceed the values established by the European legislation (Groundwater Directive, 2006/118/EC; EU Directive, 2020/2184) and the World Health Organization drinking water standards (WHO, 2022), except for As and SO_4^{2-} (Table 4). Concerning As, exceedances above the regulatory limit of 10 μg L^- (EU Directive, 2020/2184; WHO, 2022) occurred in few springs (e.g., S. Teresa (Cuasso al Monte) and Piattamala 1 (Tirano) shown in Fig. 3-B. According to the local water managers, the water collected from these springs is mixed with waters from surrounding springs showing lower As concentrations in order to be distributed to the population for drinking purposes (LarioReti, personal communication). SO_4^{2-} maximum exceedances occurred in Fonte del Drago (Oltre il Colle, Fig. 5), showing values around 965 mg L^- (regulatory limit: 250 mg L^-; EU Directive, 2020/2184). For this reason, this spring is neither linked to the municipal aqueduct nor is used for drinking purposes.

The spatial distribution of physical parameters, major and minor ions highlighted the different hydrochemical characteristics of springs related to the groundwater circulation within the various geological formations (Fig. 4). The electrical conductivity summarises the concentration of the major anions, as high electrical conductivity values are correlated to high concentrations of sulphates and calcium, and vice-versa. Thus, the electrical conductivity distribution clearly reflects the two main geological domains: i) low electrical conductivity values (EC < 231 μS cm^{-1}) reflect a groundwater circulation in metamorphic, other crystalline and clastic rocks; ii) medium-to-high electrical conductivity values (231 μS cm^{-1} < EC < 716 μS cm^{-1}) reflect a groundwater circulation in calcareous and dolomitic rocks (Fig. S3 in the Supplementary Material); iii) very high electrical conductivity values (EC > 716 μS cm^{-1}) reflect groundwater circulation through limestones, claystones and evaporites, due to high concentrations of sulphates.

An interesting aspect is the presence of high nitrate concentrations (NO_3^- > 15 mg L^-) in springs characterised by shallow groundwater flow systems, recognised as those springs showing an average temperature higher than 12 °C or in the range between 6 °C and 12 °C and a temperature variation higher than ± 2 °C during the monitoring period. This result may indicate a groundwater contamination due to the presence of anthropogenic sources (e.g., leakages from the sewage system) within the recharge area of the springs, worsened by the reduced protection of the aquifer system. Such hypothesis is also supported by the correlation between nitrates and chlorides (Fig. S4 in the Supplementary Material), as the presence of chlorides in groundwater is usually related to the contamination due to anthropogenic sources (e.g., leakages from the sewage system, road salt; Howard, 1997; Vázquez-Suñé et al., 2005).

The spatial distribution of arsenic concentrations reflects the presence of crystalline silicate rocks (i.e., granitoid and metasedimentary gneisses, amphibolites). In fact, As concentrations are generally very low and below the regulatory limit for drinking purposes, however those few springs showing concentrations exceeding the established regulatory limit (As > 10 μg L^-; EU Directive, 2020/2184; WHO, 2022) are in correspondence of crystalline silicate rocks or glacial deposits bearing abundant clasts of the same lithotypes (Pfeifer et al., 2002).

The isotope ratios $\delta^{18}O$ – δ^2H analyses show that the selected springs distribution fits well with the Global Meteoric Water Line (GMWL, Craig et al., 1961) and two Local Meteoric Water Lines valid for Northern Italy (Longinelli and Selmo, 2003; Giustini et al., 2016), highlighting the

Table 4
Statistics of the main physico-chemical and hydrochemical parameters monitored by ARPA Lombardia. Statistics on the average values measured in the period 2014–2018.

Parameter	Unit	Arithmetic mean	Minimum	Median	Maximum	Standard deviation
Temperature	°C	9.89	3.68	9.71	14.70	2.48
pH	To 20 °C	7.52	6.52	7.57	7.93	0.29
Electrical conductivity	To 20 °C, μS/cm	332.58	50.63	290.50	1626.17	239.67
Water hardness	mg/L	187.21	21.50	157.33	1119.17	163.23
Ca^{2+}	mg/L	50.32	4.35	41.08	401.42	53.04
Mg^{2+}	mg/L	12.58	1.58	12.47	38.75	8.23
K^{+}	mg/L	1.19	0.35	0.84	4.18	0.81
Na^{+}	mg/L	3.01	0.50	1.86	12.83	2.76
Cl^{-}	mg/L	3.96	0.56	1.64	17.75	4.51
F^{-}	μg/L	315.27	125.00	293.75	682.00	113.54
SO_4^{2-}	mg/L	43.38	2.11	14.94	964.00	128.80
HCO_3^{-}	mg/L	162.38	17.25	166.50	453.23	97.79
NO_3^{-}	mg/L	7.54	0.94	4.67	26.17	6.54
NH_4^{+}	μg/L	31.14	20.00	26.25	90.00	13.63
As	μg/L	2.46	1.00	1.00	41.93	5.62
Fe	μg/L	12.67	5.00	10.00	41.88	6.32
Zn	μg/L	20.86	4.25	20.00	77.22	11.74

meteoric origin of groundwater (Fig. 5-A). These results are in good agreement with previous studies on local sectors of the study area (Peña-Reyes et al., 2015; Sacchi et al., 2019; Citrini et al., 2021; Sbarbati et al., 2021). The distribution of samples in the $\delta^{18}O$ – $\delta^{2}H$ plot also agrees with the prevailing meteoric circulation from SW to NE. There is a general enrichment in light isotopes from the southern to the northern sectors where springs are mostly located at higher altitudes.

The existence of three vertical isotope gradients ($\Delta\delta^{18}O$/100 m) in the literature (two reported in Longinelli and Selmo, 2003; one in Minissale and Vaselli, 2011) allows determing an approximate range of elevation for the main recharge areas of the monitored springs (Fig. 5-B). The three vertical isotope gradients do not cover the entire extension of the study area and their reliability decreases out of the bounds of their validity range, limited to a maximum elevation of 2250 m a.s.l. Thus, the elevation of the recharge area might be over- or underestimated and a comparison with the elevation of the surrounding mountainous ridges and peaks, the geomorphological, geological and structural characteristics of the area is necessary. In 27 cases out of 31 sampled springs the range of elevation is coherent with the elevation of the surrounding mountainous ridges and peaks. For two of these springs, the result is also validated by tracer tests conducted in 1989 and 1990 in the surrounding karst areas (Tognini et al., 2011). In the other four cases, the range of elevation is higher than the maximum elevation of the surrounding ridges and peaks. A possible explanation is the mixture of meteoric water with stream or snowmelt water infiltrating uphill of the spring (Filippini et al., 2018). After their validation, these data were used to further validate the delimitation of groundwater bodies considering that the recharge area of the spring must be contained within the same groundwater body where the spring is located (see Section 4.3 further on).

4.3. Groundwater bodies

Sixteen groundwater bodies have been identified in the study area (Fig. 6-A) following the procedure summarized in Section 2.2, Section 3.3 and according to Masetti et al. (2022). Five groundwater bodies were recognised in the northern sector (Pennine and Austroalpine nappes North of the Insubric Line) and 11 in the southern sector (Southern Alps fold-and-thrust belt). Table 5 reports a summary of their characteristics in terms of areal extension, groundwater budget components, number of springs within Regione Lombardia and ARPA Lombardia networks and distribution of the Dominant Flow Characteristics (as defined in Table 1). Over the 9975 km^2 studied domain (lakes excluded), an average inflow of 1.68 $m^3\ y^{-1}\ m^{-2}$ related to precipitation is calculated. Average outflows due to evapotranspiration, streamflow discharge and groundwater withdrawals are equal to 0.57, 1.02 and 0.05 $m^3\ y^{-1}\ m^{-2}$, respectively. Considering average inflows and outflows, an uncertainty equal to +0.05 $m^3\ y^{-1}\ m^{-2}$ is calculated. It is worthy of note that some groundwater bodies are delimited also by non-natural boundaries (national and regional administrative borders), thus their areal extension might be underestimated.

According to the criteria defined in Section 3.3, a validation process followed the delimitation of each groundwater body, by evaluating: i) its consistency with previous local and regional studies, ii) the agreement of hydrochemical data of groundwater with the lithological characteristics within each groundwater body, iii) the uncertainty in groundwater budget. As an example for groundwater body 11, Fig. 6-B summarises all the available information considered for the validation process: over the plan-view of the 3D model, spring location and their discharge, main and minor caves location, flow direction derived from speleological surveys (also confirmed through tracer tests) and derived information from isotope analysis (recharge areas) are plotted. Considering that a groundwater body should be a hydrogeological independent volume, with no significant groundwater exchange with the surrounding bodies, we observe that: a) the results of speleological activities are fully consistent with this feature, by clearly indicating how vectors indicating the flow direction are fully contained within the groundwater body; b) the elevation range of the recharge area for the two monitored springs, identified through isotope analysis, is in excellent agreement with the elevation of the mountainous sector in the area where the most relevant caves are located. For groundwater body 11, the groundwater budget estimates an uncertainty term equal to +0.11 $m^3\ y^{-1}\ m^{-2}$ (Table 5), including the systemic error in the evaluation of the variables and a potential surplus amount in (ground) water resources.

5. Discussion

All the groundwater bodies (GWBs) located in the northern sector (1–5, hosted by metamorphic nappes mostly north of the Insubric Line) show a low GW exploitation (never higher than 0.04 $Mm^3\ y^{-1}\ km^{-2}$) coupled with a negative uncertainty term. The former can be considered a property related to the main geological features of the area, characterised by crystalline basement units containing fractured aquifers with low-medium hydraulic conductivity values. GWB 1 is the exception, constituted by carbonate rocks. In this case, the low GW values can be explained by the boundary of the body, represented by administrative limits, which could have excluded springs located outside of Lombardy Region. The negative uncertainty terms, which are close to zero, could indicate a balance between groundwater recharge and actual exploitation needs, if not an impoverishing of the resource. Conversely, larger negative values could be related to some errors in the calculation of the water budget terms due to some non-natural boundaries of these five

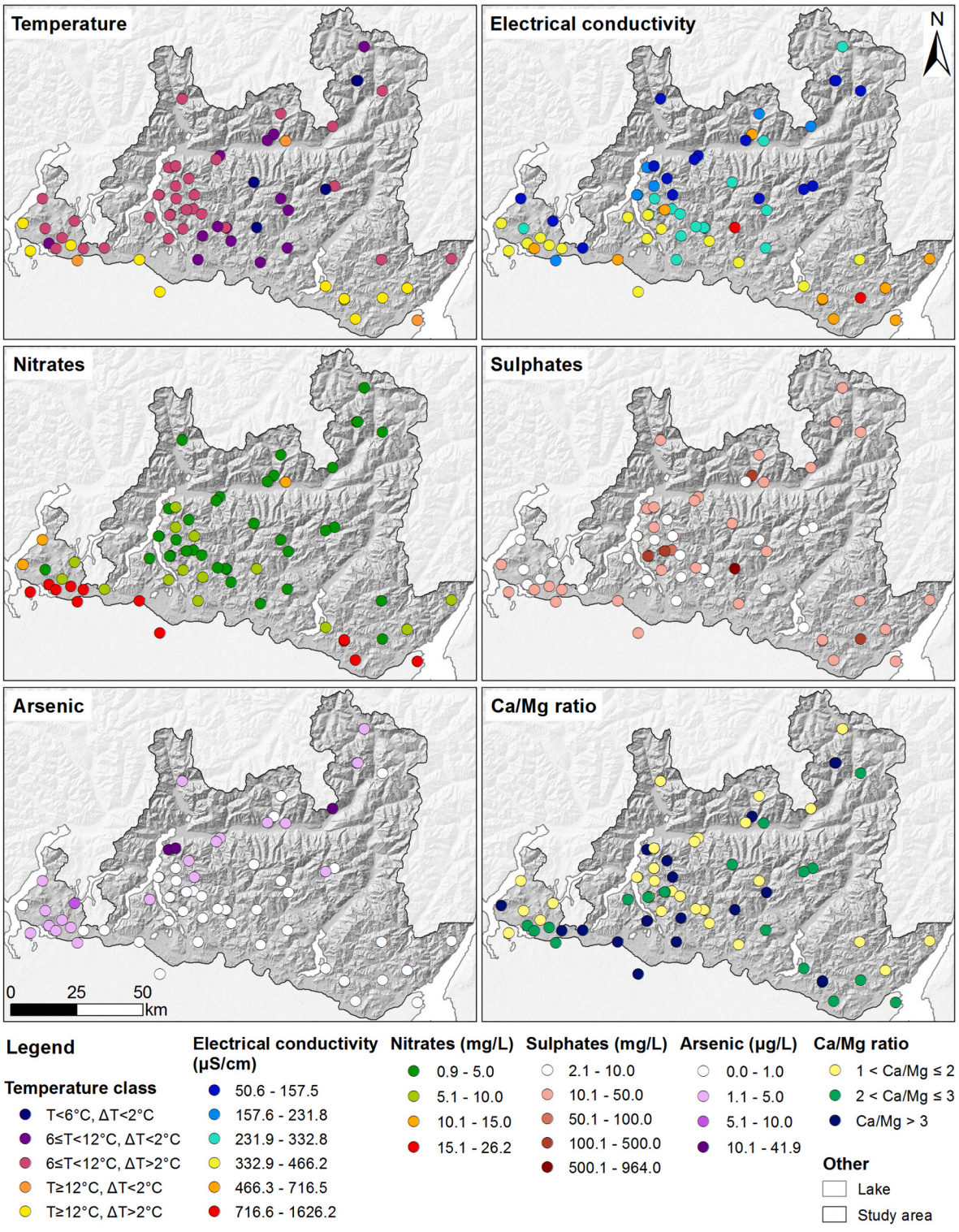

Fig. 4. Main hydrochemical features, average values for the 2014–2018 monitoring period. Basemap: hillshade; source: https://osm-wms.de/.

GWBs. All of them have a part of their boundaries that is represented by the administrative limit of Lombardy Region; therefore, they could represent only a part of a larger GWB.

In the southern sector, the groundwater exploitation is much larger, with the exceptions related to those GWBs widely characterised by Southalpine basement units (GWBs 6, 14) and clastic formations (GWB 8, 15, 16). In addition, the uncertainty term for the Southern Alps GWBs is usually positive, with just two exceptions (GWBs 7 and 16), again for two GWBs with part of their boundaries represented by administrative limits. Anyway, the positive uncertainty terms could suggest a renewal of the resource and a possible groundwater availability larger than its actual exploitation.

Groundwater bodies 7, 11, 12, 13 are the most productive and they are all located in the Southalpine carbonate aquifers of the southern sector, while 1, 5, 15, 16 are the less productive ones; their productivity is six times lower than in GWB 11. The ratio GW/(P-ET) can be interpreted as an index of sustainability of groundwater resources. It shows the lowest value for GWB 1, 5, 6 and 10 that makes GWB 5 as the most

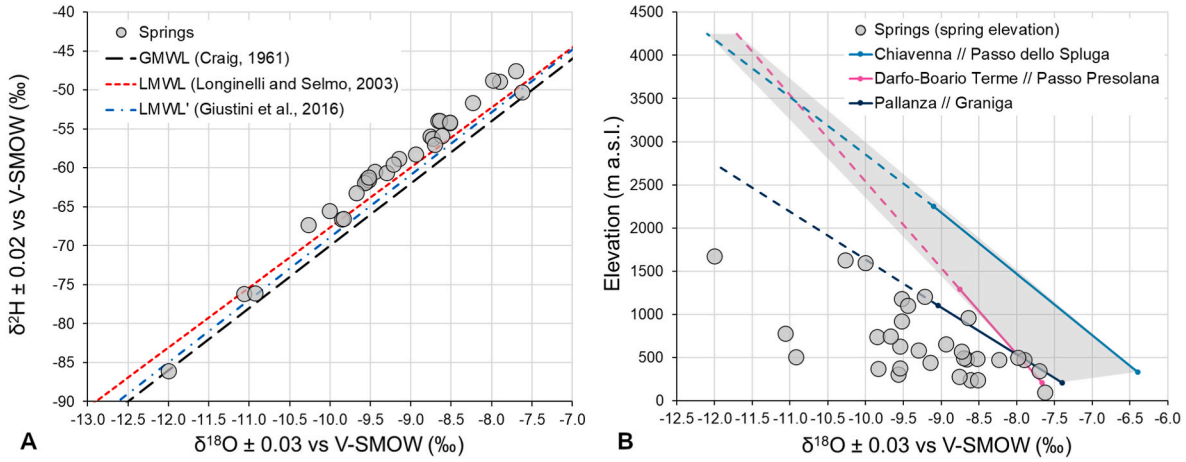

Fig. 5. A) $\delta^{18}O$ – $\delta^{2}H$ diagram for the selected springs with the Global Meteoric Water Line (GMWL, Craig et al., 1961) and two Local Meteoric Water Lines valid for Northern Italy: LMWL (Longinelli and Selmo, 2003) and LMWL' (Giustini et al., 2016). B) $\delta^{18}O$ – elevation diagram for the selected springs with the three vertical isotope gradients reported in the legend as "Location of the meteorological station at the lower elevation//Location of the meteorological station at the higher elevation" and represented by the dots on the respective lines. Chiavenna//Passo dello Spluga from Minissale and Vaselli (2011); Darfo-Boario Terme//Passo Presolana and Pallanza//Graniga from Longinelli and Selmo (2003). Solid line: validity range of the gradient. Dashed line: linear extrapolation. Grey shadow area: range of elevation of the recharge areas of the selected springs.

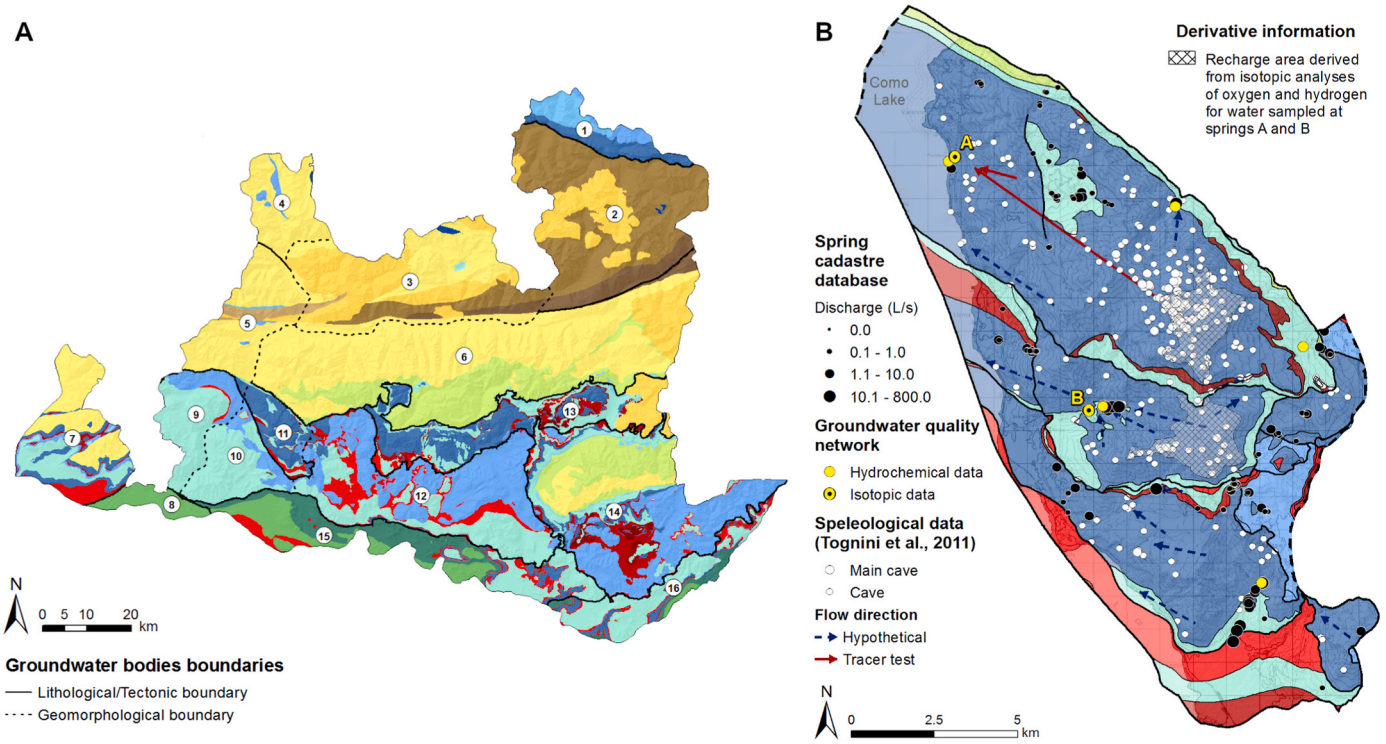

Fig. 6. A) Groundwater bodies identified in the Alps of Lombardy. B) Sketch of the groundwater body 11, with the related hydrogeological information, including the identification of the possible recharge areas of two springs where $\delta^{18}O$ – $\delta^{2}H$ were determined. Basemap: 1:50,000 scale Lombardy Region Technical Map (https://www.geoportale.regione.lombardia.it/).

critical GWB in terms of sustainability, due to the combination of low recharge (P-ET), low GW resource and negative uncertainty terms. Conversely, the highest index values are for GWBs 7,11, 12, 13, which are the most exploited too. These data identify GWB 13 as the most important groundwater resource in the area: the strategical relevance of this GWB is also highlighted by the high positive uncertainty terms (which could include a volume of GW storage not exploited) and by the huge extension of the GWB.

Perico et al. (2022) recently explored a methodology to quantify groundwater storage dynamics in snow-dominated catchments, with a high temporal and spatial resolution through the aid of remote sensing data. The catchments studied by these Authors almost coincide with the GWBs 1, 2, 3 and 6 identified in this study. Results of the groundwater budget terms for these GWBs (as summation of 1, 2, 3 and 6 components) are of the same order of magnitude of the hydrological components determined by Perico et al. (2022), representing an excellent cross-validation between regional and local scale studies in mountainous areas.

The basic analysis showing close direct correlation between NO_3^- – Cl^- in Fig. S3 (Supplementary Material) indicates an impact of anthropic

Table 5
Groundwater bodies characteristics. P: precipitation amount, including rainfall and snowmelt; ET: evapotranspiration term; SW: streamflow discharge; GW: groundwater withdrawals; ε: uncertainty term. $m^3\ y^{-1}\ m^{-2}$ is equivalent to $Mm^3\ y^{-1}\ km^{-2}$. *Groundwater bodies partly limited by national or regional administrative borders.

Id	Area (km^2)	P ($m^3\ y^{-1}\ m^{-2}$)	ET ($m^3\ y^{-1}\ m^{-2}$)	SW ($m^3\ y^{-1}\ m^{-2}$)	GW ($m^3\ y^{-1}\ m^{-2}$)	ε ($m^3\ y^{-1}\ m^{-2}$)	Number of springs of the cadastre network (Tables 2 and i)	Number of springs of the ARPA Lombardia network	Area of dominant flow characteristic (percentage of the total area)		
									Karst	Fissured	Impervious
1*	217.8	1.23	0.37	0.85	0.02	−0.01	21	1	100.0	–	–
2*	1135.71	1.33	0.42	0.95	0.04	−0.07	299	3	0.2	99.8	–
3*	979.29	1.58	0.48	1.20	0.03	−0.12	255	6	1.0	99.0	–
4*	289.26	1.60	0.44	1.22	0.03	−0.09	64	0	7.8	92.2	–
5*	390.51	1.90	0.55	1.36	0.02	−0.04	200	0	4.1	95.9	–
6	1885.05	1.85	0.50	1.04	0.03	0.27	710	11	0.3	99.7	–
7*	462.6	1.78	0.66	1.27	0.08	−0.22	213	8	43.1	44.3	12.6
8*	100.17	1.57	0.69	0.67	0.03	0.18	28	2	–	99.5	0.5
9*	260.28	1.94	0.63	1.10	0.05	0.16	170	0	97.4	0.1	2.5
10	255.6	1.86	0.65	0.98	0.03	0.20	167	2	99.5	0.2	0.3
11	149.22	2.01	0.61	1.17	0.12	0.11	144	7	87.5	1.1	11.4
12	1002.78	1.87	0.62	1.08	0.10	0.08	521	11	84.6	–	15.4
13*	635.35	2.03	0.53	1.07	0.09	0.33	177	2	69.4	15.6	15.0
14*	1235.97	1.69	0.57	1.03	0.03	0.06	305	3	57.1	29.3	13.6
15	645.21	1.38	0.69	0.66	0.02	0.01	131	2	27.2	61.3	11.5
16	351.09	1.23	0.64	0.63	0.02	−0.07	38	2	73.0	14.4	12.6

activities on groundwater. The highest values of NO_3^- are concentrated along the southern boundary of the study area, along the transition between the Pre-Alps and the Po Plain, where most of the human-related activities developed (Stevenazzi et al., 2020). Nevertheless, groundwater quality is generally quite high through all the domain, considering that the physico-chemical and hydrochemical parameters do not exceed the values established by the European and international legislation. This excellent situation has few exceptions mostly related to geogenic sources creating very few local exceedances of the regulatory limits for As and SO_4^{2-} that are constantly monitored by the Regional Environmental Authority.

The presence of a significant amount of groundwater in some GWBs, and the good water quality shows the relevant value of the GW resources in the area as Strategic Storage Reservoir. Groundwater bodies 7, 12, 13 can be considered as the most important areas for GW storage and use, considering the combination of excellent quality, high productivity, high recharge and extension. Among the three, GWB 7 could appear as a vulnerable body because of the large negative uncertainty term. However, the body boundaries consist almost exclusively of administrative limits, cutting out of the model a large recharge contributing area. Also, the body is characterised by a complex geology including the tectonic contacts between crystalline basement units and carbonate formations. In particular, crystalline basement units cover the whole northern (and higher precipitation) half of the GWB, which could be the reason for the very high streamflow (low permeability rocks with low infiltration potential). The analysis of the uncertainty term shows that also GWB 6 could represent an important asset for future water needs. The uncertainty term is quite high and the GWB is the largest in the area; the two features highlight that the GWB could have a significant storage of groundwater that is not already exploited.

The identification of GWBs indicates that the existing monitoring network is not completely efficient to provide reliable data useable for defining the quality status of groundwater bodies as required by EU directives. The main causes are: a) the monitoring points density is very low, 1 point per 166 km^2; b) the spatial distribution of the monitoring points is rather heterogeneous, GWBs 7 and 8 have about 1 point every 55 km^2 while GWBs 2, 13, 14, 15 less than 1 point per 300 km^2; c) three of the 16 GWBs do not contain any monitored spring. The need to increase the number of monitoring points is obvious, as well as the need to modify their relative distribution. The results of the study can be used to support the revision of the monitoring network by relocating some monitoring stations and adding many other stations to cover the lack of information in some sectors of the area. The aim is not to get to a spatial homogenous distribution of the monitoring stations but to: a) obtain information for all the GWBs that have been identified; b) adapt the density of monitoring stations as a function of GWB productivity and importance as a Strategic Storage Reservoir for the future; c) keep the surveillance of the geogenic sources of contamination that can locally alter groundwater quality.

For a selected number of springs (31), we identified a range of elevation for recharge areas through the combination of isotopic analyses and vertical isotope gradients. In 27 out of 31 cases the range was consistent with the geomorphological, geological and hydrogeological characteristics of the groundwater body where the springs are located. This methodological approach could be gradually extended to other springs to support a reliable identification of recharge areas, a fundamental step for the implementation of adequate protection strategies of water resources. The reliability of such approach would improve with the determination of other specific vertical isotope gradients spanning over the entire study area. With the increasing interest that water scientists and stakeholders are demonstrating towards mountain water resources (Renner et al., 2013; Blancas et al., 2018; Somers and McKenzie, 2020; Masao et al., 2022; Scanlon et al., 2023), a coordinated effort to implement regional studies (e.g., Alps) aiming at the definition of the variability of the vertical isotope gradients would be beneficial to the scientific community.

6. Conclusions

This study demonstrated the efficacy of coupling a 3D hydrostratigraphic approach with the definition of the water budget and water hydrochemical fingerprint to identify and delineate groundwater bodies at a regional scale in a geologically complex Alpine environment. The study defined the groundwater bodies according to the Water Framework Directive 2000/60/EC (European Commission, 2000) and Groundwater Directive 2006/118/EC (European Commission, 2006), assessing their quantitative and qualitative state too. The key findings can be summarized as follows.

- Qualitative and quantitative hydrogeological information allowed to translate hydrostratigraphic units into groundwater bodies.
- Groundwater bodies were validated with local independent hydrogeological information (e.g., groundwater physico-chemical characteristics, tracer tests in karst areas, $\delta^{18}O - \delta^{2}H$ analysis).

- Sixteen GWB (groundwater bodies) were identified over the 10.290 km^2 study area, five in the northern sector (about 3000 km^2) and 11 in the southern sector (about 7000 km^2).
- For each groundwater body, it was possible to evaluate the contribution of the main parameters affecting the groundwater budget and to estimate the storage capacity of the bodies.
- The Southern sector shows a groundwater storage capacity four times larger than the Northern sector.
- Groundwater quality in the study domain is generally excellent, qualifying it as an important Strategic Storage Reservoir.
- The actual groundwater monitoring network shows a non-homogeneous distribution of observation points within the GWBs, due to both under-size (e.g., GWBs 2, 13, 14, 15) and over-size (e.g., GWBs 7, 8, 11) conditions, or absence of monitoring points (i.e., GWBs 4, 5, 9).
- The combination of geological, hydrogeological, hydrochemical (including stable isotopes analysis) approaches allows a preliminary identification of recharge areas that can be proposed for some GWBs as important protection areas.

Credit author statement

Stefania Stevenazzi: Conceptualization, Methodology, Software, Validation, Formal analysis, Investigation, Data Curation, Writing Original Draft, Writing - Review & Editing, Visualization. Chiara Zuffetti: Conceptualization, Methodology, Formal analysis, Data Curation, Writing - Review & Editing, Visualization. Corrado A.S. Camera: Conceptualization, Methodology, Software, Validation, Investigation, Writing - Review & Editing, Supervision. Alice Lucchelli: Conceptualization, Methodology, Formal analysis, Investigation, Data Curation, Writing - Review & Editing. Giovanni P. Beretta: Conceptualization, Resources, Writing - Review & Editing, Supervision, Funding acquisition. Riccardo Bersezio: Conceptualization, Methodology, Validation, Resources, Writing Original Draft, Writing - Review & Editing, Supervision, Funding acquisition. Marco Masetti: Conceptualization, Methodology, Validation, Resources, Writing Original Draft, Writing - Review & Editing, Supervision, Project administration, Funding acquisition.

Declaration of competing interest

The authors declare that they have no known competing financial interests or personal relationships that could have appeared to influence the work reported in this paper.

Data availability

Data will be made available on request.

Acknowledgments

This study was partially supported by Regione Lombardia in the framework of a collaboration agreement with the Dipartimento di Scienze della Terra “A. Desio” of the Università degli Studi di Milano. The authors also thank ARPA Regione Lombardia and the local water supply companies for supporting spring water sampling.

When this study began, S. Stevenazzi was affiliated with the Dipartimento di Scienze della Terra “A. Desio” of the Università degli Studi di Milano. Authors would like to thank the two anonymous reviewers who helped improving the manuscript.

Appendix A. Supplementary data

Supplementary data to this article can be found online at https://doi.org/10.1016/j.jenvman.2023.117958.

References

Allocca, V., Manna, F., De Vita, P., 2014. Estimating annual groundwater recharge coefficient for karst aquifers of the southern Apennines (Italy). Hydrol. Earth Syst. Sci. 18 (2), 803–817. https://doi.org/10.5194/hess-18-803-2014.

Arras, C., Balia, R., Botti, P., Buttau, C., Cau, P., Da Pelo, S., Funedda, A., Ghiglieri, G., Loi, A., Lorrai, M., Melis, M.T., Testa, M., 2019. Geological criteria to the 3D delimitation of groundwater bodies (GWB) in the hydrographic district of Sardinia. Flowpath 2019 - national Meeting on Hydrogeology. In: Conference Proceedings. Ledizioni, Milano. https://doi.org/10.14672/55260121, 978-88-5526-012-1.

Ballesteros, D., Malard, A., Jeannin, P.Y., Jiménez-Sánchez, M., García-Sansegundo, J., Meléndez-Asensio, M., Sendra, G., 2015. KARSYS hydrogeological 3D modeling of alpine karst aquifers developed in geologically complex areas: Picos de Europa National Park (Spain). Environ. Earth Sci. 74 (12), 7699–7714. https://doi.org/10.1007/s12665-015-4712-0.

Beretta, G.P., 1986. Contributo per la stesura di una carta idrogeologica della Lombardia. Acque Sotterr. 4, 1–21 (Milano).

Bigi, G., Cosentino, D., Parotto, M., Sartori, D., Scandone, P., 1990. Structural model of Italy. Progetto finalizzato geodinamica CNR, sheets 1–9. Quad. Ric. Sci. 3, 114.

Blancas, A.N.I., Torre-Cuadros, M., de los, Á.L., Carrera, G.A.M., 2018. Using foresight to gain a local perspective on the future of ecosystem services in a mountain protected area in Peru. Mt. Res. Dev. 38, 192–202. https://doi.org/10.1659/MRD-JOURNAL-D-17-00090.1.

Camera, C., Bruggeman, A., Hadjinicolaou, P., Pashiardis, S., Lange, M.A., 2014. Evaluation of interpolation techniques for the creation of gridded daily precipitation (1×1 km^2); Cyprus, 1980–2010. J. Geophys. Res. Atmos. 119, 693–712. https://doi.org/10.1002/2013JD020611.

Centro Lombardo di Studi ed Iniziative per lo Sviluppo Economico, 1969. Le Risorse Idriche in Lombardia. A cura di Ugo Raffa, p. 165.

Ceriani, M., Carelli, M., 2003. Carta delle precipitazioni medie, massime e minime annue del territorio alpino della Regione Lombardia (registrate nel periodo 1891–1990). Pubblicazione Regione Lombardia.

Christensen, C.W., Hayashi, M., Bentley, L.R., 2020. Hydrogeological characterization of an alpine aquifer system in the Canadian Rocky Mountains. Hydrogeol. J. 28, 1871–1890. https://doi.org/10.1007/s10040-020-02153-7.

Ciancetti, G., Pilla, G., 2001. Indagini per la valutazione delle risorse idriche sotterranee del massiccio del Mt. Altissimo (Valle Camonica, Alpi meridionali). Memor. Soc. Geol. Ital. 56, 171–180.

Citrini, A., Camera, C.A.S., Alborghetti, F., Beretta, G.P., 2021. Karst groundwater vulnerability assessment: application of an integrative index-based approach to main catchments of middle Valseriana springs (Northern Italy). Environ. Earth Sci. 80 (17), 610. https://doi.org/10.1007/s12665-021-09860-8.

Civita, M., 2005. Idrogeologia applicata e ambientale. Casa Editrice Ambrosiana Ed., p. 736

Commissione sulle risorse idriche in acque sotterranee dell’Italia, 1982. Studio Delle Risorse in Acque Sotterranee dell’Italia, vol. 1. Th.Schafer GmbH-D-3000 Hannover, p. 193.

Craig, H., 1961. Isotopic variations in meteoric waters. Science 133 (3465), 1702–1703.

Crespi, A., Brunetti, M., Lentini, G., Maugeri, M., 2018. 1961–1990 high-resolution monthly precipitation climatologies for Italy. Int. J. Climatol. 38, 878–895. https://doi.org/10.1002/joc.5217.

Crespi, A., Brunetti, M., Ranzi, R., Tomirotti, M., Maugeri, M., 2021. A multi-century meteo-hydrological analysis for the Adda river basin (Central Alps). Part I: gridded monthly precipitation (1800–2016) records. Int. J. Climatol. 41, 162–180. https://doi.org/10.1002/joc.6614.

Deutloff, A., Burger, A., Castany, G., Gattinger, T.E., Jäckly, H., Manfredini, M., Margat, J., Mijatoviç, B., Monition, F., Traub, B., 1974. Notice explicative de la Carte Hydrogéologique Internationale de l’Europe à l’échelle 1:1.500.000. Feuille C5 Berne. Bundesanstalt für Bodenforschung (Hannover) – UNESCO, Paris), p. 96.

Domenico, P.A., Schwartz, F., 1990. Physical and Chemical Hydrogeology. Wiley, p. 824.

Dwire, K.A., Mellmann-Brown, S., Gurrieri, J.T., 2018. Potential effects of climate change on riparian areas, wetlands, and groundwater-dependent ecosystems in the Blue Mountains, Oregon, USA. Clim. Serv. Assess. Adapt. Clim. Change Blue Mt. Oregon (USA) 10, 44. https://doi.org/10.1016/j.cliser.2017.10.002.

European Commission, 2000. Directive 2000/60/EC of the European parliament and of the council of 23 october 2000 establishing a framework for community action in the field of water policy. Off. J. Eur. Commun. L327, 1–73, 22 December 2000.

European Commission, 2003. WFD CIS Guidance Document No. 2. Identification of Water Bodies. No. 92-894-5122-X. Published by the Directorate General Environment of the European Commission, Brussels. ISSN No. 1725-1087.

European Commission, 2006. Directive 2006/118/EC of the European Parliament and of the Council of 12 December 2006 on the protection of groundwater against pollution and deterioration. Off. J. Eur. Union L 372, 19–31, 27 December 2006.

European Commission, 2020. Directive (EU) 2020/2184 of the European Parliament and of the Council of 16 December 2020 on the quality of water intended for human consumption (recast). Off. J. Eur. Union L 435, 1–62, 23 December 2020.

Ferrario, A., Tognini, P., 2016. Il Catasto Speleologico Lombardo. (Progetto Tu.Pa.Ca.), p. 450.

Ferrer, J., Pérez-Martín, M.A., Jiménez, S., Estrela, T., Andreu, J., 2012. GIS-based models for water quantity and quality assessment in the Júcar River Basin, Spain, including climate change effects. Sci. Total Environ. 440, 42–59. https://doi.org/10.1016/j.scitotenv.2012.08.032.

Filippa, G., Cremonese, E., Galvagno, M., Isabellon, M., Bayle, A., Choler, P., Carlson, B. Z., Gabellani, S., Morra di Cella, U., Migliavacca, M., 2019. Climatic drivers of greening trends in the Alps. Rem. Sens. 11 (21), 2527. https://doi.org/10.3390/rs11212527.

Filippini, M., Squarzoni, G., De Waele, J., Fiorucci, A., Vigna, B., Grillo, B., Riva, A., Rossetti, S., Zini, L., Casagrande, G., Stumpp, C., Gargini, A., 2018. Differentiated spring behavior under changing hydrological conditions in an alpine karst aquifer. J. Hydrol. 556, 572–584. https://doi.org/10.1016/j.jhydrol.2017.11.040.

Gambillara, R., Terrana, S., Giussani, B., Monticelli, D., Roncoroni, S., Martin, S., 2013. Investigation of tectonically affected groundwater systems through a multidisciplinary approach. Appl. Geochem. 33, 13–24. https://doi.org/10.1016/j.apgeochem.2013.01.005.

Giustini, F., Brilli, M., Patera, A., 2016. Mapping oxygen stable isotopes of precipitation in Italy. J. Hydrol.: Reg. Stud. 8, 162–181. https://doi.org/10.1016/j.ejrh.2016.04.001.

Günther, A., Duscher, H., 2019. Extended Vector Data of the International Hydrogeological Map of Europe 1:1,500,000 (Version IHME1500 v1.2). Technical note. BGR IHME1500 Homepage 01.02.2019. https://www.bgr.bund.de/ihme1500.

Guyennon, N., Valt, M., Salerno, F., Petrangeli, A.B., Romano, E., 2019. Estimating the snow water equivalent from snow depth measurements in the Italian Alps. Cold Reg. Sci. Technol. 167, 102859. https://doi.org/10.1016/j.coldregions.2019.102859.

Hall, D.K., Riggs, G.A., 2016. MODIS/Terra Snow Cover 8-Day L3 Global 500m SIN Grid, Version 6. [subset W 8.5, S 45.5, E 11, N 47]. Boulder, Colorado USA. NASA National Snow and Ice Data Center Distributed Active Archive Center. https://doi.org/10.5067/MODIS/MOD10A2.006 access. (Accessed 22 October 2022).

Havril, T., Tóth, Á., Molson, J.W., Galsa, A., Mádl-Szőnyi, J., 2018. Impacts of predicted climate change on groundwater flow systems: can wetlands disappear due to recharge reduction? J. Hydrol. 563, 1169–1180. https://doi.org/10.1016/j.jhydrol.2017.09.020.

Hofstra, N., Haylock, M., New, M., Jones, P., Frei, C., 2008. Comparison of six methods for the interpolation of daily, European climate data. J. Geophys. Res. Atmos. 113, D21110 https://doi.org/10.1029/2008JD010100.

Horvat, B., Rubinic, J., 2006. Annual runoff estimation - an example of karstic aquifers in the transboundary region of Croatia and Slovenia. Hydrol. Sci. J. 51, 314–324. https://doi.org/10.1623/hysj.51.2.314.

Howard, K.W.F., 1997. Impacts of urban development on groundwater. In: Eyles, N. (Ed.), Environmental Geology of Urban Areas. Geotext, 3, 93–104. Special publication of the Geological Association of Canada.

IHME, 1970. International Hydrogeological Map of Europe 1:1,500,000 (IHME1500) - Sheet C5 Bern [access. https://download.bgr.de/bgr/Grundwasser/IHME1500/Beispielbild/C5_Bern.png. (Accessed 22 October 2022).

IPCC (Intergovernmental Panel on Climate Change), 2019. Special Report: the Ocean and Cryosphere in a Changing Climate (Final Draft). IPCC Summary for Policymalers: Vol. TBD (Issue TBD) access. https://www.ipcc.ch/srocc/. (Accessed 22 October 2022).

ISTAT (Istituto di Statistica Applicata al Territorio), 2019. Utilizzo e qualità della risorsa idrica in Italia, 978-88-458-1976-6, p. 104.

ISTAT (Istituto di Statistica Applicata al Territorio), 2021. Population Census on 1st January 2021 access. http://www.istat.it/. (Accessed 22 October 2022).

JAXA (Japan Aerospace Exploration Agency), 2021. ALOS Global Digital Surface Model "ALOS World 3D-30m (AW3D-30). version 3.1. access. https://www.eorc.jaxa.jp/ALOS/en/dataset/aw3d30/aw3d30_e.htm. (Accessed 22 October 2022).

Jones, D.B., Harrison, S., Anderson, K., Whalley, W.B., 2019. Rock glaciers and mountain hydrology: a review. Earth Sci. Rev. 193, 66–90. https://doi.org/10.1016/j.earscirev.2019.04.001.

Kling, H., Fuchs, M., Paulin, M., 2012. Runoff conditions in the upper Danube basin under an ensemble of climate change scenarios. J. Hydrol. 424 (425), 264–277. https://doi.org/10.1016/j.jhydrol.2012.01.011.

Legates, D.R., McCabe, G.J., 1999. Evaluating the use of "goodness-of-fit" Measures in hydrologic and hydroclimatic model validation. Water Resour. Res. 35, 233–241. https://doi.org/10.1029/1998WR900018.

Longinelli, A., Selmo, E., 2003. Isotopic composition of precipitation in Italy: a first overall map. J. Hydrol. 270 (1), 75–88. https://doi.org/10.1016/S0022-1694(02)00281-0.

Lu, J., Sun, G., McNulty, S.G., Amatya, D.M., 2005. A comparison of six potential evapotranspiration methods for regional use in the Southeastern United States 1. JAWRA J. Am. Water Resourc. Assoc. 41, 621–633. https://doi.org/10.1111/j.1752-1688.2005.tb03759.x.

Masao, C.A., Prescott, G.W., Snethlage, M.A., Urbach, D., Torre-Marin Rando, A., Molina-Venegas, R., Mollel, N.P., Hemp, C., Hemp, A., Fischer, M., 2022. Stakeholder perspectives on nature, people and sustainability at Mount Kilimanjaro. People Nat. 4, 711–729. https://doi.org/10.1002/pan3.10310.

Masetti, M., Bersezio, R., Beretta, G.P., Camera, C., Lucchelli, A., Stevenazzi, S., Zuffetti, C., 2022. Caratterizzazione dei corpi idrici sotterranei compresi nelle porzioni collinari e montane ai fini della tutela e gestione delle risorse idriche sotterranee. Technical report (in Italian). Regione Lombardia and Università degli Studi di Milano, Milano, p. 198 access. https://www.regione.lombardia.it/wps/portal/istituzionale/HP/DettaglioServizio/servizi-e-informazioni/Enti-e-Operatori/Territorio/governo-delle-acque/idromont-caratterizzazione-idrogeologica-aree-montane/idromont-caratterizzazione-idrogeologica-aree-montane. (Accessed 31 January 2023).

Maxey, G.B., 1964. Hydrostratigraphic units. J. Hydrol. 2 (2), 124–129.

McKenney, M.S., Rosenberg, N.J., 1993. Sensitivity of some potential evapotranspiration methods to climate change. Agric. For. Meteorol. 64, 81–110. https://doi.org/10.1016/0168-1923(93)90095-Y.

Medici, G., Smeraglia, L., Torabi, A., Botter, C., 2021. Review of modeling approaches to groundwater flow in deformed carbonate aquifers. Groundwater 59 (3), 334–351. https://doi.org/10.1111/gwat.13069.

Milly, P.C.D., Dunne, K.A., Vecchia, A.V., 2005. Global patterns of trends in streamflow and water availability in a changing climate. Nature 438, 347–350. https://doi.org/10.1038/nature04312.

Minissale, A., Vaselli, O., 2011. Karst springs as "natural" pluviometers: constraints on the isotopic composition of rainfall in the Apennines of central Italy. Appl. Geochem. 26 (5), 838–852. https://doi.org/10.1016/j.apgeochem.2011.02.005.

Mouton, J., Mangano, F., Fried, J.J., 1982. Studio Delle Risorse in Acque Sotterranee dell'Italia. Generaldirektion Umwelt Europäische Gemeinschaften, vol. 6. Th.Schafer GmbH. D. 3000, Hannover.

Nash, J.E., Sutcliffe, J.V., 1970. River flow forecasting through conceptual models part I – A discussion of principles. J. Hydrol. 10, 282–290. https://doi.org/10.1016/0022-1694(70)90255-6.

Parajka, J., Szolgay, J., 1998. Grid-based mapping of long-term mean annual potential and actual evapotranspiration in Slovakia, IAHS Publ. In: Proceedings of the HeadWater'98 Conference, April 1998, pp. 123–129. Merano, Italy.

Paul, F., Rastner, P., Azzoni, R.S., Diolaiuti, G., Fugazza, D., Le Bris, R., Nemec, J., Rabatel, A., Ramusovic, M., Schwaizer, G., Smiraglia, C., 2020. Glacier shrinkage in the Alps continues unabated as revealed by a new glacier inventory from Sentinel-2. Earth Syst. Sci. Data 12 (3), 1805–1821. https://doi.org/10.5194/essd-12-1805-2020.

Peeters, L., 2014. A background color scheme for piper plots to spatially visualize hydrochemical patterns. Groundwater 52 (1), 2–6. https://doi.org/10.1111/gwat.12118.

Peña Reyes, F.A., Crosta, G.B., Frattini, P., Basiricò, S., Della Pergola, R., 2015. Hydrogeochemical overview and natural arsenic occurrence in groundwater from alpine springs (upper Valtellina, Northern Italy). J. Hydrol. 529, 1530–1549. https://doi.org/10.1016/j.jhydrol.2015.08.029.

Perico, R., Brunner, P., Frattini, P., Crosta, G.B., 2022. Water balance in alpine catchments by sentinel data. Water Resour. Res. 58, e2021WR031355 https://doi.org/10.1029/2021WR031355.

Pfeifer, H.-R., Beatrizotti, G., Berthoud, J., De Rossa, M., Girardet, A., Jäggli, M., Lavanchy, J.-C., Reymond, D., Righetti, G., Schlegel, C., Schmit, V., Temgoua, E., 2002. Natural arsenic contamination of surface and ground waters in Southern Switzerland (Ticino). Bull. Appl. Geol. 7, 83–105.

Piper, A.M., 1944. A graphic procedure in the geochemical interpretation of water-analyses. Trans. Am. Geophys. Union 25 (6), 914–923.

Regione, Lombardia, 2016. Programma di Tutela e Uso delle Acque – Relazione generale, p. 388 access. https://www.regione.lombardia.it/wps/portal/istituzionale/HP/DettaglioRedazionale/servizi-e-informazioni/Enti-e-Operatori/territorio/governo-delle-acque/piano-tutela-acque-pta-2016/piano-tutela-acque-pta-2016. (Accessed 22 October 2022).

Renner, R., Schneider, F., Hohenwallner, D., Kopeinig, C., Kruse, S., Lienert, J., Link, S., Muhar, S., 2013. Meeting the challenges of transdisciplinary knowledge production for sustainable water governance. Mt. Res. Dev. 33, 234–247. https://doi.org/10.1659/MRD-JOURNAL-D-13-00002.1.

Sacchi, E., Paolucci, V., Tedesco, D., Oster, H., 2019. The "Antica Fonte" of Boario (Italy): an hydrochemical and isotopic investigation in support of mineral water development. E3S Web Conf. 98, 07027 https://doi.org/10.1051/e3sconf/20199807027.

Sánchez, D., Carrasco, F., Andreo, B., 2009. Proposed methodology to delineate bodies of groundwater according to the European water framework directive. Application in a pilot Mediterranean river basin (Málaga, Spain). J. Environ. Manag. 90 (3), 1523–1533. https://doi.org/10.1016/j.jenvman.2008.11.001.

Sauter, M., Florea, L.J., others, 2008. Focus group on karst hydrology - conceptual models, aquifer characterization, and numerical modeling. Front. Karst Res. 77–81.

Sbarbati, C., Gorla, M., Lacchini, A., Cristaldi, A., Monaco, D.L., Marinelli, V., Righetti, C., Simonetti, R., Petitta, M., Aravena, R., 2021. Multi-isotopic regional-scale screening on drinking groundwater in Lombardy Region (Italy). Acque Sotterr. - Ital. J. Groundwater 10. https://doi.org/10.7343/as-2021-501.

Scanlon, B.R., Fakhreddine, S., Rateb, A., de Graaf, I., Famiglietti, J., Gleeson, T., Grafton, R.Q., Jobbagy, E., Kebede, S., Kolusu, S.R., Konikow, L.F., Long, D., Mekonnen, M., Schmied, H.M., Mukherjee, A., MacDonald, A., Reedy, R.C., Shamsudduha, M., Simmons, C.T., Sun, A., Taylor, R.G., Villholth, K.G., Vörösmarty, C.J., Zheng, C., 2023. Global water resources and the role of groundwater in a resilient water future. Nat. Rev. Earth Environ. 4, 87–101. https://doi.org/10.1038/s43017-022-00378-6.

Schoeller, H., 1962. Les Eaux Souterraines. Mason et Cie, Paris.

Scotti, R., Brardinon, F., Alberti, S., Frattini, P., Crosta, G.B., 2013. A regional inventory of rock glaciers and protalus ramparts in the central Italian Alps. Geomorphology 186, 136–149. https://doi.org/10.1016/j.geomorph.2012.12.028.

Seibert, J., Jenicek, M., Huss, M., Ewen, T., 2015. Chapter 4 - snow and ice in the hydrosphere. In: Shroder, J.F., Haeberli, W., Whiteman, C. (Eds.), Snow and Ice-Related Hazards, Risks and Disasters. Academic Press, Boston, pp. 99–137. https://doi.org/10.1016/B978-0-12-394849-6.00004-4.

Sekulić, A., Kilibarda, M., Heuvelink, G.B.M., Nikolić, M., Bajat, B., 2020. Random forest spatial interpolation. Rem. Sens. 12, 1687. https://doi.org/10.3390/rs12101687.

Somers, L.D., McKenzie, J.M., 2020. A review of groundwater in high mountain environments. WIREs Water 7, e1475. https://doi.org/10.1002/wat2.1475.

Stevenazzi, S., Camera, C.A.S., Masetti, M., Azzoni, R.S., Ferrari, E.S., Tiepolo, M., 2020. Atmospheric nitrogen depositions in a highly human-impacted area. Water, Air, Soil Pollut. 231, 276. https://doi.org/10.1007/s11270-020-04613-y.

Struckmeyer, W.F., Margat, J., 1995. Hydrogeological Maps: a Guide and a Standard Legend. IAH - International Contributions to Hydrogeology, vol. 17. Heinz Heise Verlag, Hannover. XVI + 177 pp.

Thornton, J., Mariethoz, G., Brunner, P., 2018. A 3D geological model of a structurally complex Alpine region as a basis for interdisciplinary research. Sci. Data 5, 180238. https://doi.org/10.1038/sdata.2018.238.

Tognini, P., Montrasio, D., Pannuzzo, G., 2011. Osservatorio Delle Aree Carsiche Lombarde - Note Illustrative, p. 183.

Turc, L., 1954. Le bilan d'eau des sols: relation entre les précipitations, l'évaporation et l'écoulement. Ann. Agronom. Sér. A IV, 491–595.

Turk, J., Malard, A., Jeannin, P.-Y., Petrič, M., Gabrovšek, F., Ravbar, N., Vouillamoz, J., Slabe, T., Sordet, V., 2015. Hydrogeological characterization of groundwater storage and drainage in an alpine karst aquifer (the Kanin massif, Julian Alps). Hydrogeol. Process. 29 (8), 1986–1998. https://doi.org/10.1002/hyp.10313.

Valt, M., Guyennon, N., Salerno, F., Petrangeli, A.B., Salvatori, R., Cianfarra, P., Romano, E., 2018. Predicting new snow density in the Italian Alps: a variability analysis based on 10 years of measurements. Hydrol. Process. 32 (20), 3174–3187. https://doi.org/10.1002/hyp.13249.

Vázquez-Suñé, E., Sánchez-Vila, X., Carrera, J., 2005. Introductory review of specific factors influencing urban groundwater, an emerging branch of hydrogeology, with reference to Barcelona, Spain. Hydrogeol. J. 13 (3), 522–533. https://doi.org/10.1007/s10040-004-0360-2.

Vigna, B., Banzato, C., 2015. The hydrogeology of high-mountain carbonate areas: an example of some Alpine systems in southern Piedmont (Italy). Environ. Earth Sci. 74, 267–280. https://doi.org/10.1007/s12665-015-4308-8.

Viviroli, D., Kummu, M., Meybeck, M., Kallio, M., Wada, Y., 2020. Increasing dependence of lowland population on mountain water resources. Nat. Sustain. 3, 917–928. https://doi.org/10.1038/s41893-020-0559-9.

Volpi, G., Magri, F., Frattini, P., Crosta, G.B., Riva, F., 2017. Groundwater-driven temperature changes at thermal springs in response to recent glaciation: bormio hydrothermal system, Central Italian Alps. Hydrogeol. J. 25 (7), 1967–1984. https://doi.org/10.1007/s10040-017-1600-6.

Welch, L.A., Allen, D.M., 2014. Hydraulic conductivity characteristics in mountains and implications for conceptualizing bedrock groundwater flow. Hydrogeol. J. 22 (5), 1003–1026. https://doi.org/10.1007/s10040-014-1121-5.

WHO (World Health Organization), 2022. Guidelines for Drinking-Water Quality, 978-92-4-004506-4, fourth ed. incorporating the first and second addenda, Geneva, p. 614. Licence: CC BY-NC-SA 3.0 IGO.